Modelling FRP open-hole tensile tests in Abaqus

BSc Thesis

Jan Swinnen

Delft University of Technology

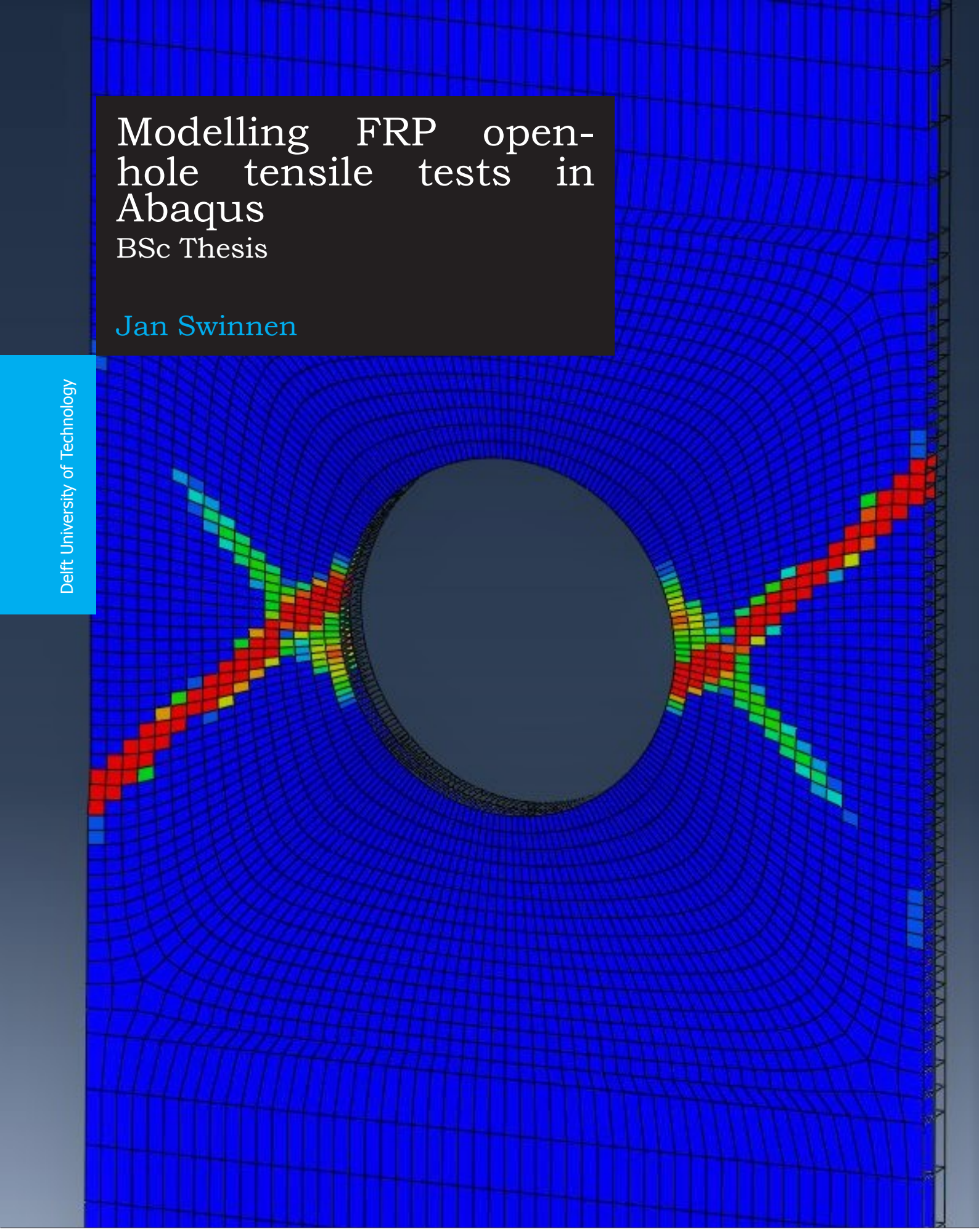

TU Delft Delft University of Technology

Challenge the future

Modelling FRP open-hole tensile tests in Abaqus

BSc Thesis

by

Jan Swinnen

in partial fulfillment of the requirements for the degree of

Bachelor of Science
in Civil Engineering

at the Delft University of Technology,
to be defended on 25th of June.

Student number: 4493575
Project duration: 23 April 2018, 2012 – 25 June 2018
Thesis committee:

Dr. M. Pavlovic,	TU Delft, supervisor
Dr. ir. F.P. van der Meer,	TU Delft, supervisor
Dr. ir. P.C.J. Hoogenboom,	TU Delft, coordinator

TU Delft Delft University of Technology

Abstract

The use of fibre reinforced polymers (FRP) are stimulated in the construction industry for their remarkable corrosion resistance, good thermo-mechanical properties, high strength-to-weight ratio and high stiffness-to-weight ratio. The open-hole strength of FRP is an important parameter in a composite design because it can be representative in simple features of composite components leading to stress concentrations such as cutouts, fastener holes or a flaw in the material. Therefore, an open-hole tension test is simulated in the finite element program ABAQUS to determine the failure load of an $[45°/-45°]$ lay-up using the material AS4/PEEK.
In ABAQUS, both static implicit and dynamic explicit analysis are performed. For both analyses, the failure loads, stability and failure mechanisms are examined. The geometry and material properties are chosen to match the properties used in van der Meer and Sluys [1] in order to compare results. The model is build up of 8808 SC8R elements and the interface between the plies is modelled using the surface-based cohesive behaviour technique.

The static and dynamic analysis revealed that there's a large influence of non-physical and time related variables on the simulated failure load of the laminate. The results of the dynamic target time step sensitivity analysis didn't converge to a legitimate value for the failure loads. The same has been concluded for the mesh size sensitivity analysis. Based on the stability of the solutions a reasonable value has been chosen for these variables.

Comparing the results of the static and dynamic analysis with the results of van der Meer and Sluys [1], illustrated that the failure loads differ largely. The failure mechanisms are different due to the homogenisation of the material that is fundamental to continuum models in ABAQUS. At the failure load in the static and dynamic analysis, the matrix fails under tension and shear through the whole thickness of the laminate in the same direction. This unrealistic event differs from the failure mechanism observed in van der Meer and Sluys [1].
In order to overcome the unrealistic failure behaviour in the static and dynamic analyses, XFEM modelling techniques are recommended to bridge the problem with the damage propagation direction parallel to the fibre direction.

Preface

This thesis was conducted to obtain the Civil Engineering bachelor's degree at Delft University of Technology. It will be part of continuing projects concerning the modelling of FRP joints. The subject was introduced by the Department Steel and Composite Structures to get a better understanding of modelling the cohesive behaviour in delamination of FRP composites using the Finite Element Analysis program ABAQUS.

At the start of this thesis my knowledge about composites and finite element modelling was very limited. Even though I used to repair sailing boats with fibreglass, my theoretical background was quasi nil. This also applied for the usage of the program ABAQUS.

Sincerely I want to thank my supervisors who provided patient advice and experienced guidance. Hopefully, the conclusions of this thesis will be of good use for upcoming research on this topic and the interesting field of composite structures.

Jan Swinnen
Delft, 16th of June 2018

Contents

List of Figures

List of Tables

1

Introduction

The exploration of FRP composites began in the 1960's when the aerospace and aviation industry were looking for a lightweight high-performance material. By combining fibres of high-strength and high-stiffness with low-cost, lightweight, environmental resistant polymers, a Fibre Reinforced Polymer (FRP) composite was created that performed better than the two components alone. [3] When in the 1970's FRP were commercialised and became cheaper, the material extended its applications in the automotive and marine industries. Although large scale FRP structures remain challenging to produce, countries are starting to develop construction guidelines and the European Union is even making it's first steps to implement the material in the Eurocode. [4] Nowadays FRP composites are stimulated in the construction industry because of their remarkable corrosion resistance, good thermo-mechanical properties, high strength-to-weight ratio and high stiffness-to-weight ratio. Furthermore are the recent developments of Finite Element Analysis (FEA) programs a good stimulant for the use of FRP composites in construction because of the complexity of the material that leads to extensive calculations.

Traditionally a structural design process involved making scale models, hand calculations and a lot of lengthy tests in the lab. Using FEA programs like ABAQUS, ANSYS, NASTRAN, etc. enables the engineers to conduct a virtual test and get approximate results of the response of the 'real' structure. [5] In this thesis the commercial program ABAQUS will be used. The product suite of ABAQUS is build up of three main products. ABAQUS/Standard is the general-purpose solver that will be used to solve finite element models with a traditional implicit integration scheme. ABAQUS/Explicit will provide an explicit integration scheme to solve nonlinear dynamic and quasi-static models. ABAQUS/CAE is the environment where results from ABAQUS/Standard and ABAQUS/Explicit simulations are created, submitted, monitored and evaluated.

In ABAQUS an open-hole test will be modelled to determine the open-hole strength and investigate the damage mechanism. The open-hole strength is an important parameter in the design of composite components. It can be representative in simple features of composite components leading to stress concentrations such as cutouts, fastener holes or a flaw in the material. The open-hole strength has to be compared with caution between analytical or numerical techniques (FEM) and experimental results because the strength strongly depends on the modelling technique in the FEA and the testing configuration in the experiments. [6]

The aim of this thesis is to investigate FEA modelling techniques to analyse delamination of notched composites in an open-hole tension test. Modelling techniques in ABAQUS will be discussed and as a conclusion, an advise will be given whether or not a certain modelling technique is efficient and correct. Also, the damage in the laminate will be analysed and stress-strain diagrams will be compared to prior research. [1]

In the next chapter the necessary background theory will be given to basically understand the mechanics of FRP materials related to the usage in ABAQUS. In chapter 3, the modelling technique will be elaborated. Subsequently, the models described in chapter 3 will be verified by performing several sensitivity analyses. In chapter 5, the results will be evaluated and compared to prior research. Finally in chapter 6, a conclusion will be derived from the results and additionally, recommendations will be given for future investigations on this topic.

2
Theory

In this chapter a basic introduction to the mechanical behaviour of FRP composites will be given that will be related to the usage in ABAQUS. Firstly, a brief description of the characteristics of the material will be illustrated, then the mechanical behaviour will be discussed with special attention to delamination.

2.1. Characteristics

FRP is a structural composite that consists of two phases whose mechanical performance is designed to be superior to those of the constituent phases alone. The fibres (e.g. carbon, glass, boron or aramide), acting as a reinforcement, are stiffer and stronger than the matrix surrounding them. The matrix phase provides support and protection to the fibres as well as transferring local stresses from one fibre to the other. Within each layer or ply, the fibres have a fixed orientation, they are unidirectional (UD). This gives a ply a fibre orientation that is indicated by an angle relative to the fixed reference axis. By stacking several plies together in various orientations, a laminate is created. The arrangement of the laminate indicating its ply composition with different fibre orientations is called the lay-up. In the figure below an example of a [0/-45/90/45/0] lay-up is given.

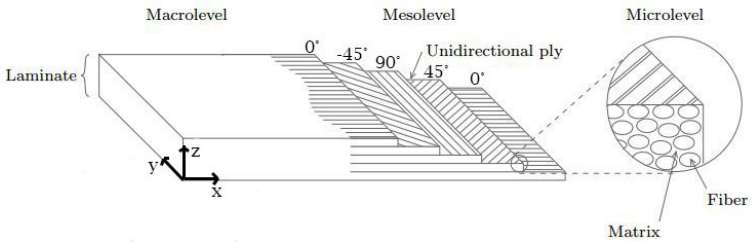

Figure 2.1: Composition of a composite laminate [2]

In ABAQUS a lay-up can be defined in two methods: create a composite section or create a composite lay-up. The composite lay-up technique enhances the definition of a composite lay-up and is especially useful when a minimal amount of sections have to be assigned with the composite definition. Because the composite section and the composite lay-up methods lead to the same results and only a few parts are needed in the model, the composite lay-up technique will be used during the modelling. [7] [8]

2.2. Unidirectional composite material behaviour

2.2.1. Elastic behaviour

The elastic behaviour of a orthotropic ply can be described by the transversely isotropic version of Hooke's law when the ply is considered stiff in fibre direction and flexible in other directions. It is defined as $\epsilon = S * \sigma$ with S the compliance matrix. For this relation, only five elastic parameters are needed instead of nine in the general stress-strain relation for orthotropic materials. (see relations in appendix A.1) [9] By making the assumption that the ply is thin, unidirectional and it will be under plane stress conditions ($\sigma_{33} = 0$, $\tau_{13} = 0$ and $\tau_{23} = 0$), the stress-strain relation is simplified and only requires four elastic parameters (E_1, E_2, ν_{12} and G_{12}). In the expression the subscript indicates the axis wherein the 1-axis is the axis in longitudinal fibre direction and the 2-axis is in the transverse direction, orthogonal to the fibre direction.

$$\begin{bmatrix} \epsilon_{11} \\ \epsilon_{22} \\ \gamma_{12} \end{bmatrix} = \begin{bmatrix} \frac{1}{E_1} & \frac{-\nu_{12}}{E_1} & 0 \\ \frac{-\nu_{12}}{E_1} & \frac{1}{E_2} & 0 \\ 0 & 0 & \frac{1}{G_{12}} \end{bmatrix} \begin{bmatrix} \sigma_{11} \\ \sigma_{22} \\ \tau_{12} \end{bmatrix}$$

This expression is used in ABAQUS to define the orthotropic elasticity under plane stress-conditions. It's still necessary to input the elastic parameters G_{13} and G_{23} because they me be required to compute transverse shear deformations in a ply. [10]

2.2.2. Failure behaviour

Currently the optimal use of FRP materials is held back due to the hard prediction of their strength and damage tolerances. To guarantee the safety of a composite structure, expensive tests and certification is needed. The challenge of today is to create models that can replace certain 'real' test. This will help engineers to have more freedom in the design process and also make optimisation of structures or components easier. The problematic aspect of analysing laminate failure is that different failure mechanisms may occur, leading to different results. In general three different failure mechanisms can be distinguished in a composite laminate. (see figure 2.2)

- **Matrix cracking** is normally the first nonlinear failure mechanism to be observed in the laminate. Small cracks develop through the thickness of the ply, between the fibres. In a multi-directional laminate this cracking usually doesn't lead to the global failure of the laminate because the fibres in different plies can still work together if the plies are still connected. It can also occur that matrix crack develop in the load direction, namely splitting cracks. They can be seen in the top ply in figure 2.2.

- **Delamination** occurs when the interface between plies fails and is a consequence of the load redistribution after matrix cracking. As this load redistribution takes place through the interface between the plies, it leads to stress concentrations in the interface. If the stress concentrations exceed the strength of the interface layer, it will cause the interface to separate and plies will lose their connection with neighbouring plies.
  If major delamination takes place in the laminate, it will lose its structural integrity and it obtains the weak resistance to forces others than in the fibre direction like in a unidirectional ply.

- **Fibre failure** is a complex failure mechanism because it can trigger different types of failure mechanisms in their vicinity. When a fibre breaks it can result in either a transverse matrix cracking when the matrix is brittle and has a good bonding with the fibres or the debonding of the fibre and the matrix in the case where the interface between fibre and matrix is rather weak and when the fibres have a relatively high ultimate strain. The breaking of the fibre is accompanied with a great release of stored energy and can cause the neighbouring fibres and matrix to fail. Most of the time this will lead to the failure of the whole composite.

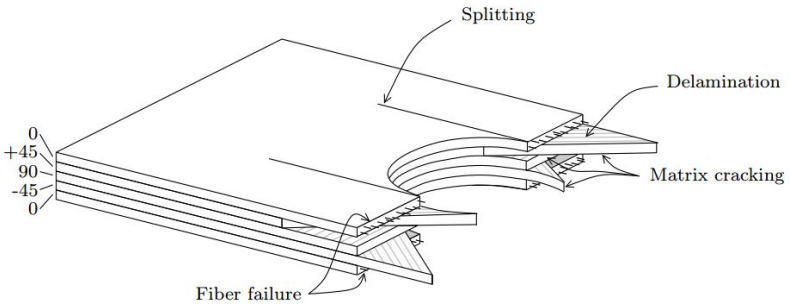

Figure 2.2: Different failure mechanisms in an tensile open-hole test [2]

2.2.3. Failure criteria

Over the past decades, many researchers have been investigating the formulation of failure criteria for unidirectional composites. The basic question is: how can we predict failure initiation due to a specified state of stress in the material? At microlevel, the aspects of failure are very complex and would lead to little hope to this question on the basis of micromechanical methods. Therefore many failure criteria are based on macrovariables, such as average stresses and strains.

Research done by Tsai in 1965 was one of the first contributions to this subject. He assumed that the failure criterion for a unidirectional composite has the same mathematical form as the one from an orthotropic plastic material. [11] [9] The disadvantage of this form was that it didn't take isotropic stresses into account. Hoffman solved this problem by adding linear stress terms to the criterion made by Tsai.
A few years later Tsai and Wu developed the Tsai-Wu criterion that is still being used today because of it's simplicity. [12] The interactive criterion for a subject under plane stress is written as:

$$\sigma_{11}\left(\frac{1}{f_{1t}}-\frac{1}{f_{1c}}\right)+\sigma_{22}\left(\frac{1}{f_{2t}}-\frac{1}{f_{2c}}\right)+\frac{\sigma_{11}^2}{f_{1c}f_{1t}}-\frac{\sigma_{11}\sigma_{22}}{\sqrt{f_{1c}f_{1t}f_{2c}f_{2t}}}+\frac{\sigma_{22}^2}{f_{2c}f_{2t}}+\frac{\tau_{12}^2}{f_{12}^2}=1$$

Altough this relatively simple equation provided a good fit with experimental data, its application and interpretation led to underlying problems. It's caused by the fact that FRP composites are build up by very dissimilar phases as mentioned in section 2.1. As a consequence, failure can occur in very different mechanism (see section 2.2.2). It is not the case that every different failure mechanism can be presented in a single smooth function as the Tsai-Wu criterion. That's why Hashin pioneered in the development of failure initiation criteria for different failure modes. [13] He distinguished four different failure mechanisms for a unidirectional composite under plane stress conditions:

- **Tensile fibre failure** in the fibre direction is critical when the longitudinal tension and longitudinal shear mutually weaken the material.

$$\left(\frac{\sigma_{11}}{f_{1t}}\right)^2+\left(\frac{\tau_{12}}{f_{12}}\right)^2\begin{cases}<1 & \text{no failure}\\ =1 & \text{failure}\end{cases}\quad\text{with } \sigma_{11}>0$$

- **Compressive fibre failure** normally leads to buckling or fibre kinking. Because the interaction between transverse compression is assumed negligible, it results in a simple maximum stress criterion.

$$\frac{\sigma_{11}}{f_{1c}}\begin{cases}<1 & \text{no failure}\\ =1 & \text{failure}\end{cases}\quad\text{with } \sigma_{11}<0$$

- **Tensile matrix failure** occurs when:

$$\left(\frac{\sigma_{22}}{f_{2t}}\right)^2+\left(\frac{\tau_{12}}{f_{12}}\right)^2\begin{cases}<1 & \text{no failure}\\ =1 & \text{failure}\end{cases}\quad\text{with } \sigma_{22}>0$$

- **Compressive matrix failure** has a more complex criterion. It is assumed that the transversely isotropic pressures has a larger effect than the uni-axial compressive failure stress.

$$\left(\frac{\sigma_{22}}{2f_{23}}\right)^2 + \left[\left(\frac{f_{2c}}{2f_{23}}\right)^2 - 1\right]\frac{\sigma_{22}}{f_{2c}} + \left(\frac{\tau_{12}}{f_{12}}\right)^2 \begin{cases} < 1 & \text{no failure} \\ = 1 & \text{failure} \end{cases} \quad \text{with } \sigma_{22} > 0$$

ABAQUS/CAE offers a direct input of the damage criteria of Fibre-Reinforced Composites. Up until now there's only the Hashin damage criterion to choose from. The program uses the equations above to calculate the damage initiation. The evolution of the damage is also integrated in ABAQUS/CAE and is based on the modelling approach of Camanho *et al.* [14] The approach is established on the energy dissipation during the failure process and the assumption is made that the damage is characterised by the progressive degeneration of the material stiffness, inducing the material to fail. When unloading after being in a damaged state, linear softening of the material is assumed. The input of the damage evolution law are the energies G_{ft}, G_{fc}, G_{mt} and G_{mc} that dissipate during each failure mechanism. In order to avoid mesh dependent solutions, the dissipation of energy for each failure mechanism is regularised by using the crack band model of Bazant and Oh [15].

2.3. Delamination & Cohesive behaviour

As mentioned in section 2.2.2, delamination is a failure mechanism that can seriously reduce the integrity of a component and can cause the total failure of a laminate. It is therefore important to have accurate analysis tools that can simulate delamination. Usually delamination initiates from discontinuities like matrix crack and free edges. In this thesis the delamination of a laminate consisting of two plies will be examined. For this purpose ABAQUS has typically two techniques to define the interaction between the two plies. One is using cohesive elements and the other creating a surface-based cohesive behaviour. The surface-based cohesive behaviour technique is well suited and will be described in this section. In section 3.2 a explanation is given why this modelling technique was chosen.

Surface-based cohesive behaviour provides an elementary way to model cohesive interactions with a negligibly small thickness (zero-thickness layer) using the traction-separation model. In ABAQUS, the traction-separation model firstly assumes a linear elastic behaviour, secondly damage initiation will take place and finally damage will evolve. [16]

1. The **linear elastic behaviour** is defined in terms of an elastic constitutive matrix that couples the nominal traction stresses to the nominal strains. ABAQUS supports writing the relation both for general coupled behaviour and uncoupled behaviour. For uncoupled behaviour, pure normal separation does not lead to cohesive forces in the shear directions and shear slip with no normal separation does not give rise to cohesive forces in normal direction. The stress-strain relation for the uncoupled behaviour is written as follows:

$$\begin{bmatrix} t_n \\ t_s \\ t_t \end{bmatrix} = \begin{bmatrix} K_{nn} & 0 & 0 \\ 0 & K_{ss} & 0 \\ 0 & 0 & K_{tt} \end{bmatrix} \begin{bmatrix} \epsilon_n \\ \epsilon_s \\ \epsilon_t \end{bmatrix}$$

   Wherein t_n, t_s and t_t represent respectively the nominal tractions in normal and 2 shear directions.

2. Under load conditions, at a certain point **damage initiation** will be inevitable and it marks the beginning of the degradation of the material. The degradation starts when stresses or separation exceeds a certain damage initiation criterion that is available in ABAQUS. Since the strength parameters of the materials are known, it's easier to opt for a stress criterion in stead of a separation criterion. Damage is going to initiate when the quadratic function involving the ratios of the nominal traction ratios reaches a value of 1.

$$\left(\frac{t_n}{t_n^{max}}\right)^2 + \left(\frac{t_s}{t_s^{max}}\right)^2 + \left(\frac{t_t}{t_t^{max}}\right)^2 \begin{cases} < 1 & \text{no failure} \\ = 1 & \text{failure} \end{cases}$$

3. The **damage evolution** of surface-based cohesive behaviour describes the gradual degradation of the cohesive stiffness. Like the damage evolution of unidirectional composite laminates, the

damage evolution of cohesive behaviour can also be based on energy dissipation. In addition, the damage evolution can also be specified as the effective separation at complete failure, relative to the separation at damage initiation. But since the input for the dissipated energy method is almost the same as for the UD composite materials, the dissipated energy method will be further discussed. The energy dissipated as result of the failure process is called the fracture energy. The fracture energy depends on the fracture mode. The first fracture mode is the opening of the interface in normal direction. The second and the third mode are both shearing modes respectively calling sliding and tearing. The opening fracture energy is denoted by G_n and the shearing modes are G_s and G_t.

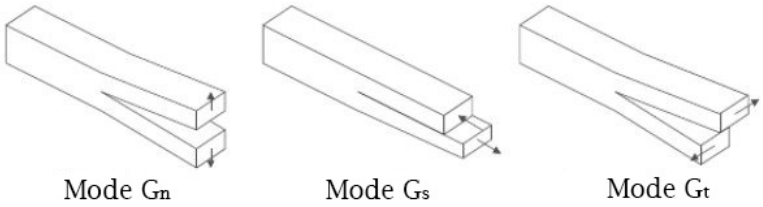

Figure 2.3: Opening, sliding and tearing fracture modes [2]

When specifying the damage evolution of a UD composite in section 2.2.2, it was also needed to specify the softening response after unloading the material. For the damage evolution of the surface-based cohesive behaviour, the same has to be done. It is also assumed that the unloading from a damaged state (point C in figure 2.4) follows a linear path back to the origin of the traction-separation curve. The area under the curve is equal to the fracture energy.

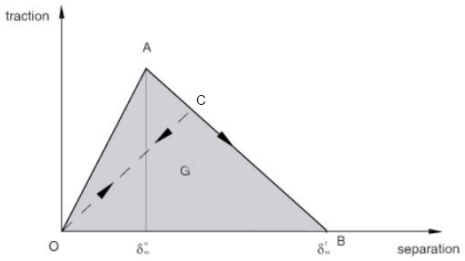

Figure 2.4: Linear damage evolution for a single mode

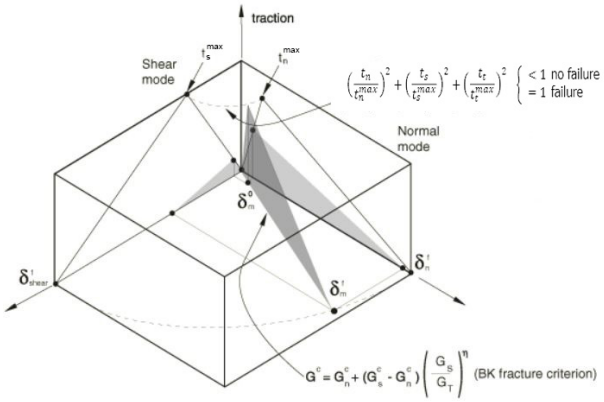

Figure 2.5: Mixed-mode response in cohesive behaviour

In figure 2.5 the vertical axis shows the traction and the two horizontal axis the magnitudes of the normal and shear separations. This makes it possible to illustrate the damage response under a mix of failure modes. The light grey triangles represent the response under pure normal and pure shear deformation. The combination of these two failure modes is represented in the dark grey triangle. The mixed mode damage evolution behaviour is controlled by the energy-based Benzeggagh-Kenane criterion. This criterion is particularly useful when the fracture energies G_s and G_t are the same. The fracture energy is calculated by:

$$G_n^C + (G_s^C - G_n^C)\left(\frac{G_{Shear}}{G_T}\right)^{\eta} = G^C$$

Where $G_{Shear} = G_s + G_t$, $G_T = G_n + G_{Shear}$ and $\eta = 1.8$. [17] G_n^C and G_s^C have to be specified in ABAQUS/CAE.
ABAQUS also offers the energy-based power law criterion but research done by Camanho *et al.* [18] proved that this law can lead to inadequate results in a small range of mode mixtures.

3
Model

The goal of this chapter is to clarify the chosen modelling techniques. The chapter starts with a short introduction of finite element modelling, followed by the modelling approach where the used techniques, material properties and geometry will be elaborated.

3.1. Finite Element Modelling

As mentioned in the introduction 1, it is important to handle the results of finite element models with caution because they may depend strongly on the modelling technique. The finite element method uses numerical solving techniques to approximate any given physical phenomenon. Partial differential equations, used to describe many space- and time dependent physical laws, are being solved with numerical model equations instead of analytically.
The finite element method is best understood from its practical application, namely finite element analysis. In reality, the number of unknowns to compute the response of a physical problem are infinite in a continuum. When performing a finite element analysis, the complex problem is discretised in to a finite number of elements. Creating the elements is called mesh generation and can be done with several shapes, like in figure 3.1. When the number of elements is increased, the results of the analysis is more likely to have accurate results although the CPU time will be higher due to more calculations. This is why it's more efficient to create a denser mesh in the region of interest.

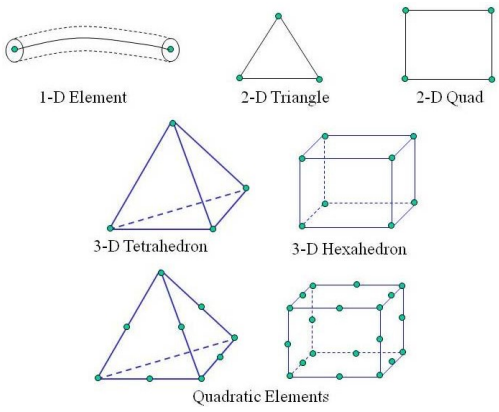

Figure 3.1: Element types

3.2. Modelling approach

To model the delamination of fibre reinforced composites, an open-hole tension test is used. The model will be build up from two deformable unidirectional continuum shells consisting of a $[45°/-45°]$ lay-up with a hole $\emptyset = 6.24$mm in the middle of the laminate. The geometry is given in figure 3.2 and is chosen based one the model used in the simulations done by van der Meer and Sluys [1]. The choice of using shell elements is simply because the thickness of the of the plies (0.5mm) is relatively small relative to the width and length (16x38.4mm) of the plies. The continuum elements discretise the entire 3D-body while conventional shell elements only a reference surface. The nodes of the continuum elements have a displacement degree of freedom only, use linear interpolation and can be loaded for static or dynamic procedures. They allow finite membrane deformation, thickness changes and large rotations, which makes them very suitable for non-linear geometric analysis like in the case of this thesis.

The material properties listed in table 3.1 are chosen to match the same properties as in van der Meer and Sluys [1]. Material parameters ($E_1, E_2, \nu_{12}, G_{12}, G_{23}$) for orthotropic elasticity come from Camanho *et al.* [18]. The transverse tensile strength, shear strength and fracture toughness parameters for the interface elements ($f_{2t}, \tau_{12}, \tau_{23}, G_2$) are also taken from Camanho *et al.* [18]. The longitudinal strengths, transverse compressive strength parameters (f_{1t}, f_{1c}, f_{2c}) are derived from Gaurav [19].

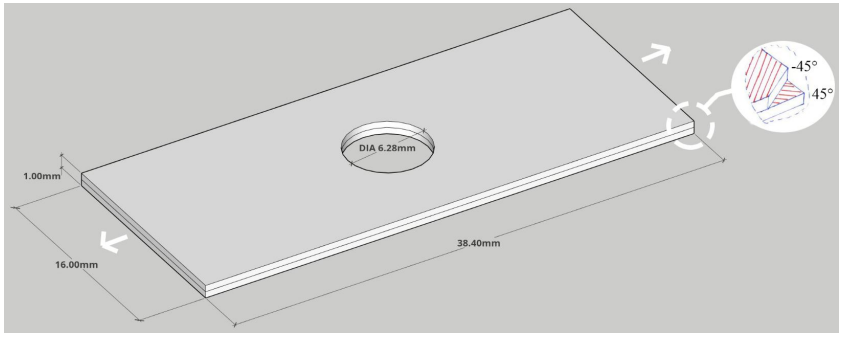

Figure 3.2: Specimen geometry

Table 3.1: Material properties AS4/PEEK

	Property	AS4/PEEK	Unity
	Density	1.885E-006	$\frac{N*s^2}{m^4}$
Elasticity	Longitudinal modulus, E_1	122.7	GPa
	Transverse modulus, E_2	10.1	GPa
	Poisson's ratio, ν_{12}	0.25	GPa
	Shear modulus, $G_{12} = G_{13}$	5.5	GPa
	Shear modulus, G_{23}	3.6	GPa
Hashin damage	Longitudinal tensile strength, f_{1t}	1020	MPa
	Longitudinal compressive strength, f_{1c}	600	MPa
	Transverse tensile strength, f_{2t}	80	MPa
	Transverse compressive strength, f_{2c}	140	MPa
	Longitudinal shear strength, f_{12}	100	MPa
	Transverse shear strength, f_{23}	100	MPa
Damage Evolution	Longitudinal fracture energy, G_1	100	$\frac{N}{mm}$
	Transverse fracture energy, G_2	0.969	$\frac{N}{mm}$
Damage stabilisation	Viscosity coefficient in longitudinal direction	0.001	MPa*s
	Viscosity coefficient in transverse direction	0.005	MPa*s

As discussed in section 2.3, the surface-based cohesive behaviour technique will be used to define the interface between the two plies. Another technique is to use cohesive elements where the cohesive properties are defined as a material property, not a interaction property.

Cohesive elements and surface-based cohesive behaviour are similar in terms of function but the latter is more easily to define since the properties are just defined to a set of interacting surfaces and no other elements have to be created. If the interface has a negligibly small thickness, the surface-based cohesive behaviour has shown to be advantageous. [20] When modelling an adhesive layer with a finite thickness and macroscopic properties, it will be more appropriate to use cohesive elements. Surface-based cohesive behaviour can also be used to model two sticky surfaces that are able to rebond during the analysis. Since the delamination of FRP materials doesn't involve rebonding, this function has to be disabled. In table 3.2, the cohesive properties are presented. They also match the properties of van der Meer and Sluys [1].

Table 3.2: Cohesive properties

Cohesive law	Property	Value	Unit
Damage initiation variables	Normal only	80	MPa
	Shear-1 only	100	MPa
	Shear-2 only	100	MPa
Damage evolution variables	Normal fracture energy	0.969	N/mm
	1^{th} shear fracture energy	1.719	N/mm
	2^{th} shear fracture energy	1.719	N/mm
Viscosity	Viscosity coefficient	0.005	MPa*s

The model is meshed with 8808 SC8R linear hexahedral elements. The mesh is coarse at the sides of the clamps and finer around the square region of interest around the hole. (see figure 3.3). The coarse and fine elements at the hole have respectively an approximate size of 0.1x1mm and 0.1x0.1mm. To ensure that the plies were meshed with one element through thickness, the sweep technique had to be used with the medial axis algorithm.

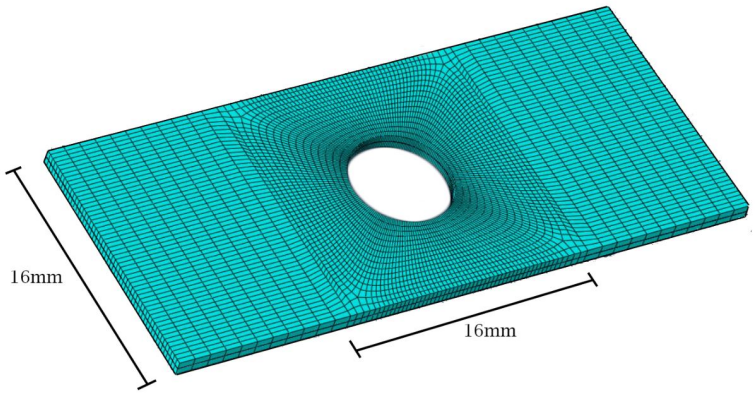

Figure 3.3: Specimen mesh

It's important to define good boundary and force application conditions since they can affect the results. The specimen is on one side fully clamped, prevented in rotations and translations in every direction. On the other side, a longitudinal displacement is applied. In displacement-controlled testing, the displacement changes incrementally while the reaction force results from the stiffness of the structure. The opposite is force-controlled testing where the load changes incrementally and the displacement results from the stiffness of the structure. Composites are usually tested with the displacement-controlled method so the ultimate strength can be easily determined by the peak in the force-displacement diagram. Additionally, the displacement-controlled method can be very useful when monitoring progressive failure. [21] Damages gradually accumulate until the final displacement results in a failure cascade which reduces the stiffness of the specimen considerably. When using the force-controlled method the model can easily become unstable when the ultimate load is suddenly reached.

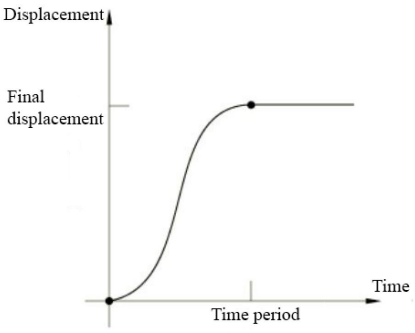

Figure 3.4: Smoothstep function

For this last reason a displacement of 0.5mm will be applied to the other side of the specimen in longitudinal direction. The other directions and rotations will be clamped.
When assigning the displacement boundary condition, it's also necessary to define at which amplitude the displacement applied. In this analysis, all the displacements are applied using the smoothstep function. This will prevent high kinetic energies and inertial effects on the dynamic explicit model.

Both implicit and explicit solvers of ABAQUS will be used to calculate the results. The implicit solver is implemented in ABAQUS/Standard and the explicit logically in ABAQUS/Explicit. ABAQUS/Standard is capable of solving linear and smooth nonlinear problems in static and quasi-static events. ABAQUS/Explicit is suitable for highly nonlinear and dynamic events. However, there are certain static or quasi-static problems for which ABAQUS/Explicit has proven to be advantageous. Typically these problems involve contact or material complexities causing convergence difficulties in ABAQUS/Standard. In ABAQUS/Standard, such analysis are computationally expensive since they require a large set of linear equations to be solved.

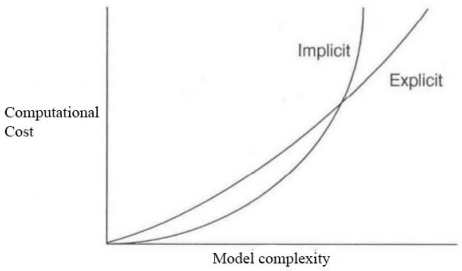

Figure 3.5: Comparison computational cost

Whereas ABAQUS/Standard needs to iterate to determine the solution of a nonlinear problem, ABAQUS/Explicit finds the solution without iterating by advancing explicitly the kinematic state of the previous increment. Even tough the same analysis requires many time increments with ABAQUS/Explicit, the analysis can be more efficient using the explicit method because the implicit method may require a large number of iterations. With the implicit method the solution is approximated by using the Newton-Raphson method and the linearised system of equations needs to be solved many times. This can cause long CPU times while convergence is not guaranteed for highly nonlinear problems. Contrarily, the explicit method doesn't need convergence checks but very small time steps are required to maintain the stability limit. A stable time step size has to be chosen so that it is smaller then the minimum time that a dilatational wave moves across an element in the model. It's calculated by:

$$\Delta t \leq l_{element} * \sqrt{\frac{\rho}{E}}$$

where Δt is the stable time increment, $l_{element}$ is the length of the element, ρ the density of the material and E the Young's modulus.
For the Dynamic, Explicit model, semi-automatic mass scaling is introduced on the whole model. Mass scaling provides a solution to run models in a shorter time with acceptable sacrifice of the accuracy of the quasi-static solution. It's a widely used and effective method for models where the velocities are low and the kinetic energy is small relative to the internal energy. The mass scaling is done by increasing the density of the smallest elements. This will lead to a larger possible stable time increment for the numerical solution of the dynamic system and therefore a shorter CPU time. The target time increment is set to 0.01 seconds.

When using an implicit solver such as ABAQUS/Standard to solve material models showing softening behaviour and stiffness degradation often lead to severe convergence difficulties. The sudden change of stiffness at the ultimate load and the subsequent negative softening cause these convergence problems. A widely used numerical stability control technique to overcome such difficulties is using viscous regularisation of the constitutive equations.
Both the traction-separation laws and the Hashin damage evolution can be regularised by using viscosity. (see value in table 3.1 and 3.2) The higher the viscosity parameter is chosen, while providing better convergence, the larger the effects on the results. For the traction-separation laws, the regularisation can permit stresses to be outside the limits set by the traction separation law. The effects of the viscosity parameter have to be validated by further reducing the value until the influence is negligibly small.

The step procedures used in ABAQUS/Standard and ABAQUS/Explicit are respectively Static, General (SG) and Dynamic, Explicit. The time period (TP) is for both analysis 1000 seconds and nonlinear effects of large deformations and displacements are enabled. Since ABAQUS has a reliable automated incrementation tool, this will be used with a minimum increment size of $1e^{-8}$.

4
Verification

The two models described in the previous chapter, i.e. Static, General and Dynamic, Explicit, need to be verified. This will be done in this chapter by analysing the effects of time variables, non-physical variables and boundary conditions on the results. For these analyses, 2 main factors are being observed. Firstly, the failure load and secondly, the stability of the dynamic analyses. The stability of the dynamic analyses is checked by plotting a diagram that visualises the difference between the applied force and the reaction force at the clamped side, relative to this reaction force. These graphs are only plotted until the point of failure to avoid noise coming from post-failure dynamic responses. Optimal stability is reached when the applied force minus the reaction force is equal to 0.
The goal of these analyses is to visualise if gradually changing a variable leads to convergence of the results.

4.1. Time variables

At the end of section 3.2, the time variables for the static and dynamic models were elaborated. Below in table 4.1, a small summary is given. In this section, the chosen time variables are analysed. The non-physical parameters, element size and viscosity, are kept constant as characterised in 3.2.

Table 4.1: Time variables

Time variable	Static, General	Dynamic, Explicit
Time period	1000s	1000s
Incrementation	Automatically	Automatically
Mass scaling: target time step	/	0.01s

4.1.1. Static General: time period sensitivity analysis

For the Static, General analysis, the time period of the test is the only time variable that has to be chosen. The time period is the time over which the total displacement of 0.5mm will be spread. As discussed in section 3.2, a smoothstep function will be used to apply the displacement. Attention has to be paid to the frequency of the function since this has to be the same as the used time period.
To investigate whether or not the time period has an influence on the failure load, a variety of time periods will be used. In figure 4.1, the failure load is plotted against the time periods. The x-axis is logarithmically scaled because time periods of 1, 10, 100 and 1000 seconds were used. This representation clearly visualises the effect of the time period. Taking the time period in the order of thousand seconds leads to convergence of the failure load. For this reason a time period of 1000 seconds is an appropriate time period for the simulation.
The force-displacement graphs can be found in appendix A.2.1. All analyses apart from the 1s analysis, aborted due to convergence errors even when the minimal time increment is set to $1e^{-8}$.

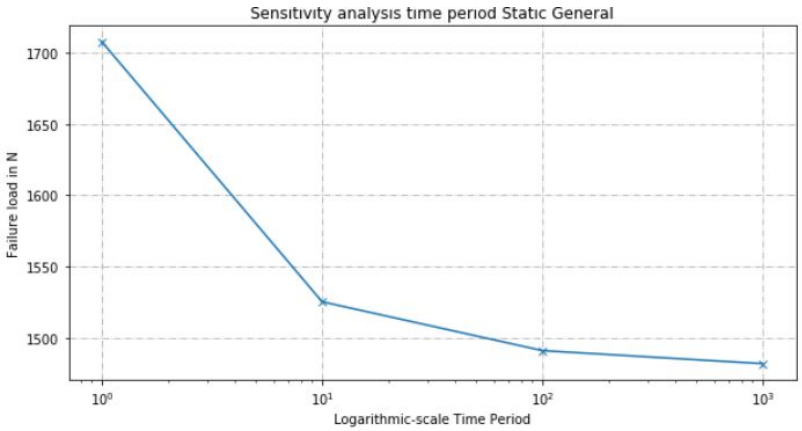

Figure 4.1: Sensitivity analysis time period

4.1.2. Dynamic, Explicit: Time step sensitivity analysis

In the dynamic analysis, time has a bigger role because inertial effects can not be ignored. Therefore, choosing the right time step is of major importance. Taking the time step too big, will lead to great inertial effects and while taking a very small time step leads to long CPU times and unstable solutions. For example, in figure A.2 it can be seen that taking a time step of 0.5s, leads to very poor results due to large inertial effects and taking the time step of 0.001s (CPU time 17 hours), leads to an unstable solution in the elastic phase of the model. For this reason, they are not taken into account in further analyses.
In the figure 4.2, the failure load is plotted against the time step. From this graph it is apparent that a linear correlation exists between the time step and failure load. Taking a larger time step leads to a larger failure load. The highest failure load is 1707 N (TS = 0.1) while the lowest is 1580 N (TS = 0.005), 10% difference.
Furthermore, it can be concluded that there's no convergence in the solutions. So from this point of view, not a single time step is the most accurate solution.

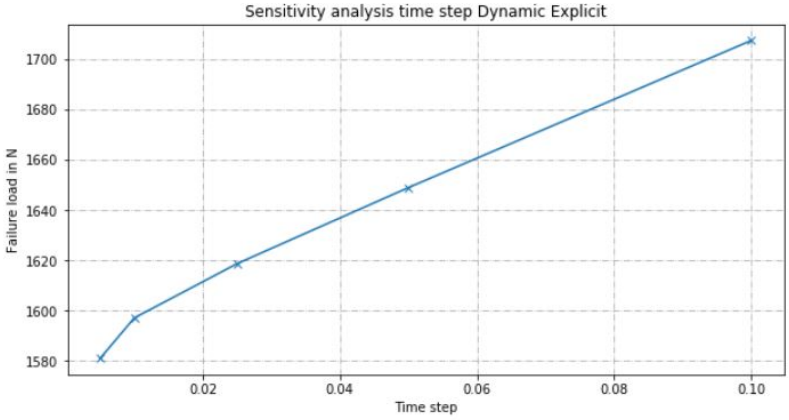

Figure 4.2: Sensitivity analysis time step

By analysing the stability of the analyses the most stable solution can be found. In figure A.3 a stability analysis is conducted as described in the beginning of this chapter. It's noticeable that large time steps in the range 0.1-0.025s suffer from inertial effects when the displacement is applied. This graph also shows that the solution with the time step set to 0.001s suffers from great instability. This can possibly be explained by the numerical round-off errors, resulting in high frequency effects in the results. When taking the time step in the range of 0.005-0.01s, the solution tends to be very stable in the beginning of the elastic phase but halfway through the elastic part the 0.005s analysis looses it's stability while the 0.01s solution stays around stable until failure.

For this reason the most stable solution, taking the time step as 0.01s, is now assumed to have the proper parameters to continue further analyses.

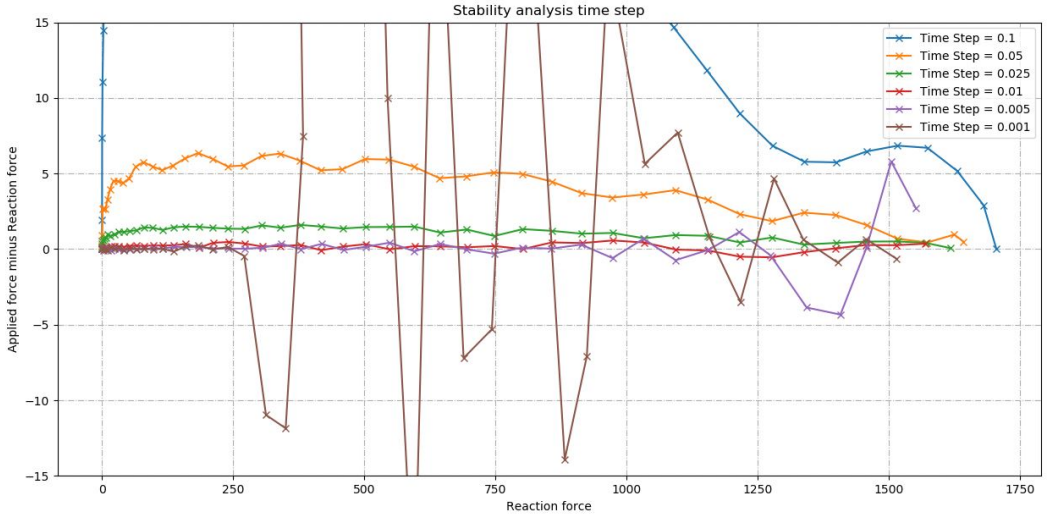

Figure 4.3: Stability analysis time step

4.1.3. Dynamic, Explicit: Time period/time step sensitivity analysis

A brief sensitivity analysis is performed on the time period in the dynamic analysis. When conducting this analysis the ratio $\frac{Time\ period}{Time\ step}$ is kept constant. This is done to ensure stable solutions, as proven in section 4.1.2. The ratio $\frac{1000}{0.01} = 100000$ is the basis of the analysis. The ratio's $\frac{100}{0.001}$, $\frac{500}{0.05}$ $\frac{1500}{0.015}$ and $\frac{2000}{0.02}$ are further analysed.

From graph 4.4, it's clear that the time period has almost no effect on the failure load. The failure load from 100s compared to 1000s is 0.25% higher, so negligibly small. The force-displacement diagram given in appendix A.2.3, reassures that the solutions are stable for all the analyses. It can be concluded from this analysis that taking a time period of 1000s and a time step of 0.01s as time variables for the dynamic analysis, leads to a good approximation of an accurate modelling technique.

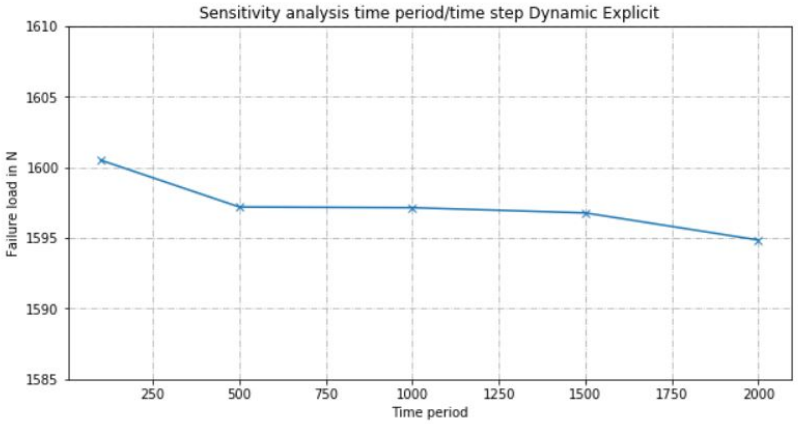

Figure 4.4: Sensitivity analysis time period/time step

4.2. Non-physical variables

For the previous analyses on the time variables, the mesh size and viscosity were kept as fixed variables. In this section, non-physical variables such as the mesh size and the viscosity, will be varied with the time variables constant as given in table 4.1.

4.2.1. Mesh size sensitivity analysis

In the beginning of chapter 3, a small introduction to Finite Element Modelling 3.1 was given. To discretise the complex problem of the laminate in the open hole-tension test, the model is meshed like in figure 3.3. In general, a finer mesh will lead to more accurate results but the CPU time will increase subsequently. To find a mesh that adequately balances accuracy and CPU time, a mesh size sensitivity analysis is performed.

As described in section 3.2, the model will have a dense mesh in the area of interest around the hole (because the stresses are significantly higher) and a coarser mesh at the constraints. For the mesh size sensitivity analysis five different mesh sizes are used. The table 4.2 below gives a summary of the approximate element sizes of the elements close to the hole and at the constraints, respectively dense and coarse mesh. In appendix A.2.4, the five different meshes are visualised.

Table 4.2: Summary element sizes

Mesh name	Dense mesh in mm	Coarse mesh in mm	No. of elements	Figure appendix
0.05	0.05x0.05	0.05x1	53192	A.4
0.07	0.07x0.07	0.07x1	17472	A.5
0.1	0.1x0.1	0.1x1	8808	A.6
0.12	0.12x0.12	0.12x1	5888	A.7
0.15	0.15x0.15	0.15x1	2872	A.8

For the Static, General solutions, all the mesh sizes ran at a viscosity of 0.005 MPa*s up until the moment just after failure or further. At small mesh sizes (0.05 & 0.07), the analyses were aborted just after failure due to convergence errors. The Dynamic, Explicit analyses experience instability problems. As can be seen in figure A.9 (Appendix A.2.4), results of the dense 0.05 and coarse 0.15 mesh sizes exhibited instability relative to the other solutions. When observing nonlinear problems, a finer mesh leads to a larger stiffness matrix and therefore the solution may lead to oscillations and divergence due to the derived unbalanced forces generated to the model during the Dynamic, Explicit analysis. Trying to run the 0.05 mesh size analysis at 2^{nd} order accuracy also led to the same unstable solutions. Due to the instability of the 0.05 and 0.15 Dynamic, Explicit solutions, they are left out of the mesh size sensitivity analysis.

In figure 4.5, the failure loads for the explicit and static (both time period of 10s and 1000s), are plotted against the mesh size. One of the first observations from the graph is that there's a clear linear trend. Choosing a denser mesh will result in a higher failure load than a coarse mesh. It's also apparent that the linear trends for different analysis are parallel. The difference between the parallel lines can be explained from different reasons.

- The different failure loads between Static, General TP=1000 and Dynamic, Explicit is caused by the variance in failure loads due to the time step in the dynamic analysis. As discussed in section 4.1.2, there was no convergence in the results of the failure load, but taking the time step at 0.01 gave the most stable results. The difference is about 120 N or 8%.
- The difference between the two static solutions is due to viscosity. In short, this is because viscosity has a strong effect on the results when taking lower time steps in static analyses. In the next section 4.2.2, a more elaborated explanation will be given.

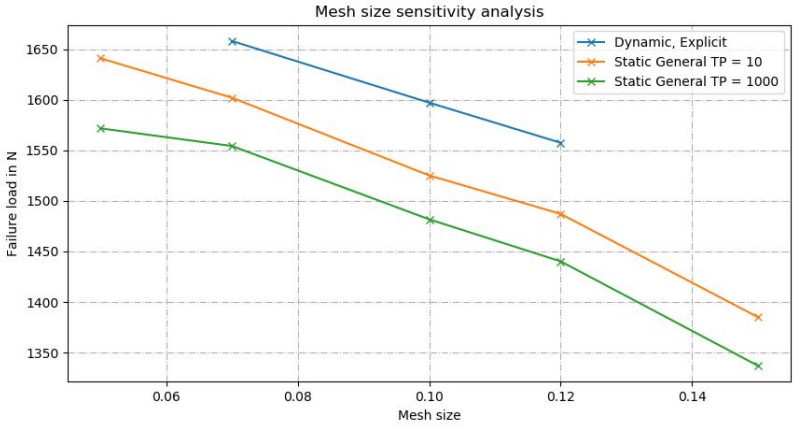

Figure 4.5: Stability analysis mesh size (TP = Time Period)

Observing the graphs clarifies that there's no clear convergence of the results. The Static, General TP=1000 analysis tends to converge for the 0.05 mesh size but this is just for one data point. The downward trend in the graphs is probably caused by an influence of viscosity regularisation related to the crack band method from Bazant and Oh [15]. This causes bigger elements to loose their stiffness quicker than smaller elements.

4.2.2. Viscosity coefficients sensitivity analysis

The end of section 3.2 described why viscous regularisation of the constitutive equations is sometimes necessary to ensure that the static solution will not lead to convergence errors. The viscosity permits stresses to be outside the limits set by the traction-separation law or the Hashin criteria. The viscosity coefficient for the stabilisation of the traction-separation law and the Hashin damage criteria are varied simultaneously between 0.001 and 0.005 MPa*s. As can bee seen in figure 4.6, the viscosity has no effect on the dynamic analyses and the static analyses with a large time period $TP \geq 1000$.

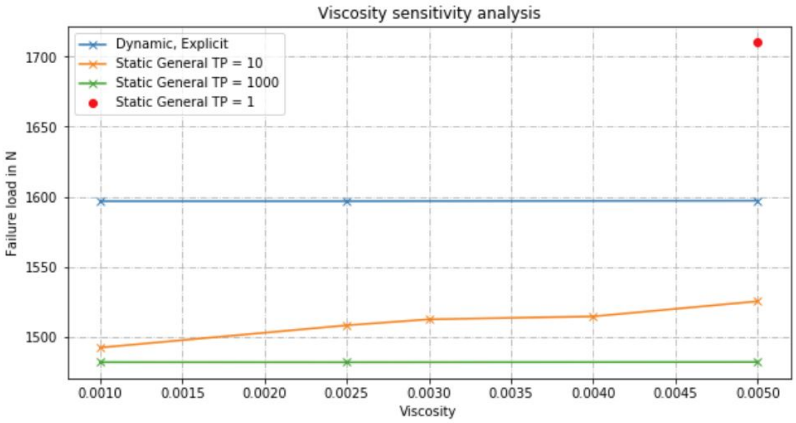

Figure 4.6: Stability analysis viscosity (TP = Time Period)

From this figure it is now clear that the failure loads of the Static, General solution are largely dependent on the viscosity parameter. This is why in section 4.1.1, the failure loads converge to a time period of 1000 seconds. Normally the failure load would be equal for different time periods without viscous regularisation. The regularisation involves the definition of a viscous stiffness degradation parameter D_v which is calculated by the damage evolution equation,

$$\dot{D_v} = \frac{1}{\mu}(D - D_v)$$

with μ the viscosity parameter and D the damage variable in the non-viscous backbone model.

The time period is linked through the damage response of the material:

$$\mathbf{t} = (1 - D_v)\bar{\mathbf{t}}$$

Basically the goal of the regularisation is that the solution of the viscous model will approximate the non-viscous model as $\frac{TP}{\mu} \Longrightarrow \infty$.
In the cases where the time period is between 1 and 100s, the fraction $\frac{TP}{\mu}$ is too big and leads to over-regularisation. Taking the fraction $\frac{TP}{\mu} = \frac{1000}{0.005} = 200000$ will lead to results where viscosity has no influence on the results. To confirm this statement, a brief analysis with ratio's $\frac{100}{0.0005}$, $\frac{10}{0.00005}$ and $\frac{1}{0.000005}$ was conducted. The results of the failure loads are all the same as can be seen in figure 4.7.

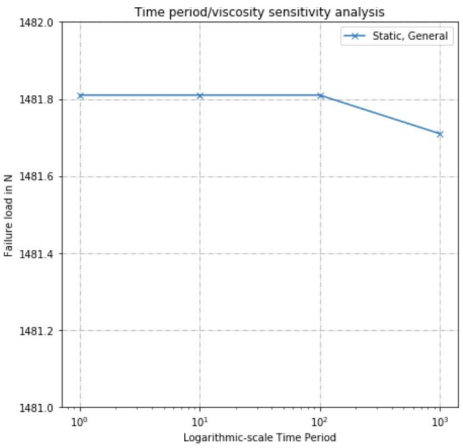

Figure 4.7: Comparison computational cost

4.3. Boundary conditions

In the previous analyses the plate was fully clamped, prevented from rotations and translations, and at the other side a displacement in pulling direction was applied of 0.5mm. The other directions were also clamped. To test whether the boundary condition has a significant influence on the failure load, a simulation with symmetry boundary conditions was conducted. The symmetry boundary conditions consists of four different boundaries. Firstly, the fixed surface is only prevented from translating in pulling direction. Secondly, one edge of the fixed surface is prevented from translation in transverse direction. Lastly, the outer surface of the bottom ply is blocked from translating in out-of-plane direction. And lastly, the pulling surface is displaced 0.5mm in pulling direction without any clamping in other direction. This boundary condition is called a symmetry boundary condition because it represents a $[45°/-45°/-45°/45°]$ lay-up, similar to what been used in van der Meer and Sluys [1].

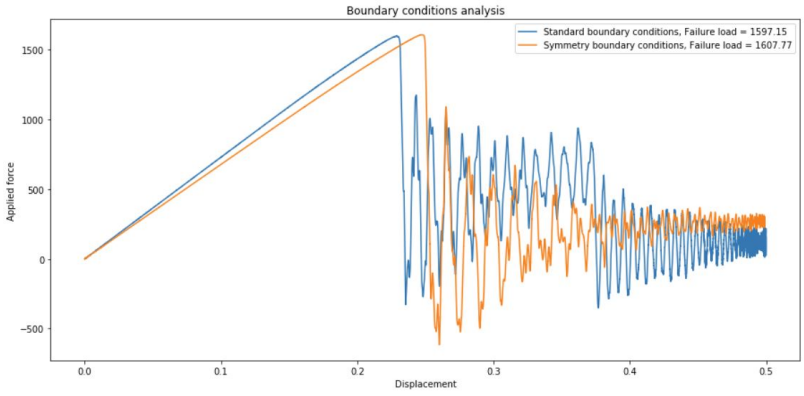

Figure 4.8: Boundary conditions analysis

From figure 4.8 it can be concluded that for both boundary conditions the failure load is the approximately the same. The difference in stiffness is due to the application of different constraints. The pulling surface is not restrained from moving in transverse direction for the symmetry boundary condition making the response less stiff than the standard boundary condition.

5
Results

In the previous chapter the Static, General and Dynamic, Explicit models, as described in chapter 3, were verified. In this chapter the solutions of these two models will be analysed and compared with results from van der Meer and Sluys [1]. Firstly, the force-displacement diagrams of the static and dynamic solutions will be compared and the differences will be explained. Secondly, the failure progress of the models will be described and visualised. At last, the force-displacement diagrams will be compared to the research from van der Meer and Sluys [1].

5.1. Static, General vs. Dynamic, Explicit

In figure 5.1, both force displacement diagrams of the static and dynamic analyses are plotted. Observing the graph it is clear that both analyses have the same stiffness (±7200 N/mm^2) but different failure loads where the dynamic analysis overshoots the static analysis. For the analyses, the same modelling parameters have been used apart from the target time step of the dynamic analysis. In both models, the viscosity (set to $\mu = 0.005$ MPa*s) and the time period ($TP = 1000$s) have no influences on the results, when changed under the ratio $\frac{TP}{\mu} = 200000$. Section 4.2.1 clarified that no convergence was taking place when changing the mesh size. For both models, the failure load decreased in parallel and linearly when increasing the mesh size. Therefore, the difference in failure load can be explained by the target time step in the dynamic analysis. Figure 4.3 makes clear that taking a time step < 0.01, leads to lower failure loads but great instability near failure. If these instabilities could be regularised it's possible that for smaller time steps in the order of thousands of a second, the results could converge.
Relatively the failure load of the dynamic analysis is 115 N or 7.78% higher than from the static analysis.

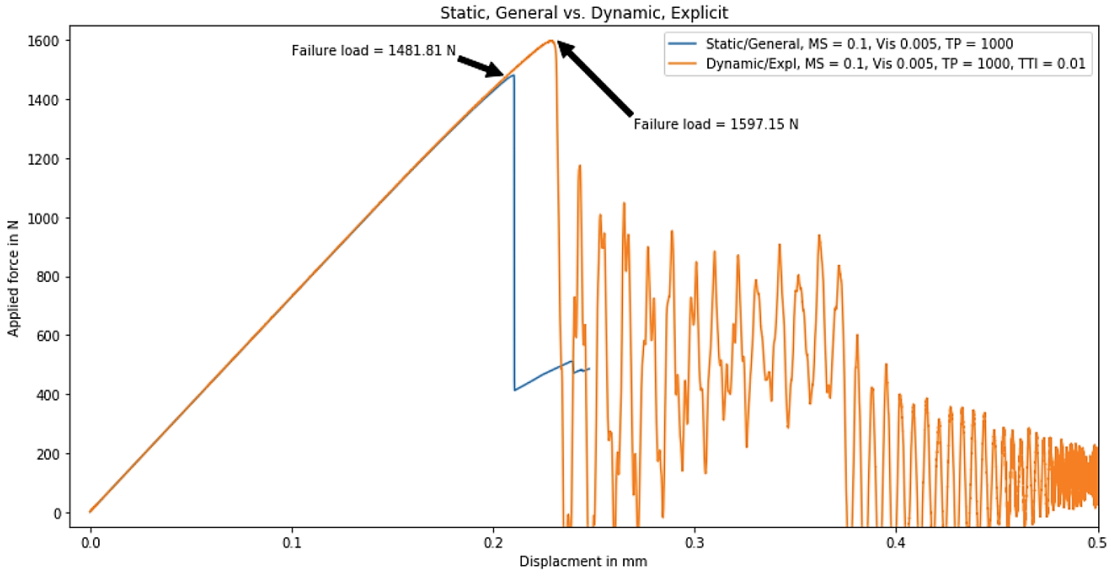

Figure 5.1: Force-displacement diagram: Static vs. Dynamic

5.2. Failure process

The failure processes of the Static, General and Dynamic, Explicit analyses are very alike. The only difference is that in the static analysis the failure initiates earlier. Because the static analysis is aborted just after failure, the failure process of the dynamic analysis is chosen to be further analysed.
To visualise the failure process, the matrix tensile (MT) damage and the cohesive surface (CS) damage are extracted from ABAQUS. The MT damage represents the failure of the plies and the CS damage shows the delamination. Both damage outputs are scaled from 0 (blue: no damage) to 1 (red: full damage).

In figure 5.3, the damage process is displayed from the initiation until the moment where the failure load is reached. Figure A.11 in appendix A.3 shows when the frame is taken on the force-displacement graph. The first damage initiates at a load of 1154.74 N and displacement 0.158709mm, exactly at the edge of the hole (see figure 5.3a). This can be logically explained by the stresses that are concentrated at the inner edge of the hole. When further increasing the load until the failure load of 1597.15 N, the MT damage grows in the shape of a triangle and the delamination continues along the edge of the hole. At the moment of failure, the matrix fails under tension and shear in a $45°$ or $-45°$ direction throughout the whole thickness of the lamina.
Previously, the orientation of the plies was never mentioned. This is because the damage occurs throughout the whole laminate, which is unrealistic. If the damage is oriented in the $45°$ direction, it's orthogonal to the fibre direction of the $-45°$ ply, which in reality can not occur. This is a consequence of the homogenisation of the material that is fundamental to continuum models. In homogenised models, the damage will always propagate in the direction where the stresses are the highest, but in reality the matrix tensile damage will spread in fibre direction through the thickness of the ply.

In the case of the $[45°, -45°]$ lay-up, matrix tensile damage will occur in one of the two plies, either in $45°$ or $-45°$ fibre direction. (figure 5.2a) This cracking between the fibres is a relatively brittle mechanism that leads to the redistribution of stresses to the other ply, through shear stresses. In reality this causes a band of shear failure orthogonal to the fibre direction in the other ply with fibres still crossing the band. (figure 5.2b) These crossing fibres still give stiffness to the material and accordingly the failure mechanism is more ductile. (figure 5.2c) However, in the continuum models in ABAQUS, this last failure mechanism can not happen. Both mechanisms are represented with a softening shear band with the same local stress-strain relation for both plies. [2] This is why after the failure load the laminate looses it's stiffness completely.

After reaching the failure load, the model shows a very dynamic response. This is probably due to the sudden release of energy which is not constrained in out-of-plane direction. After a displacement of 0.397772mm, a second damage band occurs orthogonal to the first damage band which runs also through the entire thickness of the laminate. Figure A.12 in appendix A.3 visualises the damage progress after the failure load.

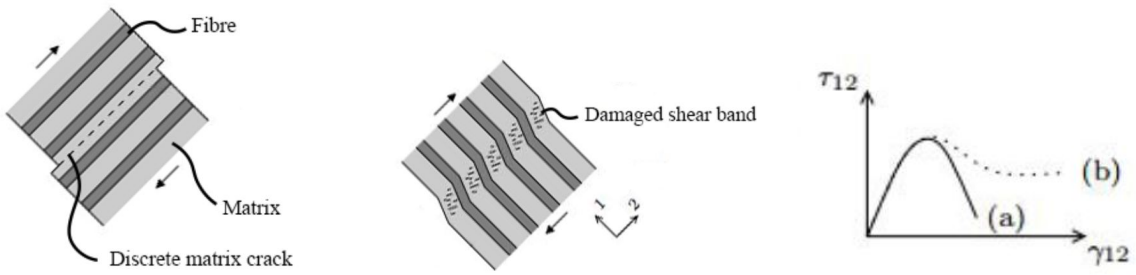

(a) (b) (c)

Figure 5.2: Matrix failure in fibre direction (a) and matrix shear failure in a band crossed by fibres (b) difference in stress-strain response (c) [2]

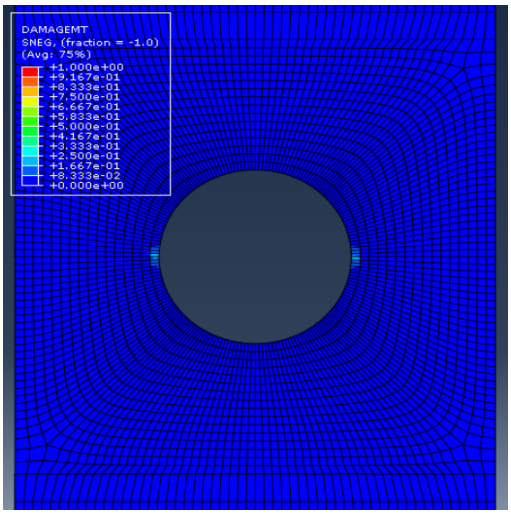

(a) MT damage, Displacement = 0.158709mm

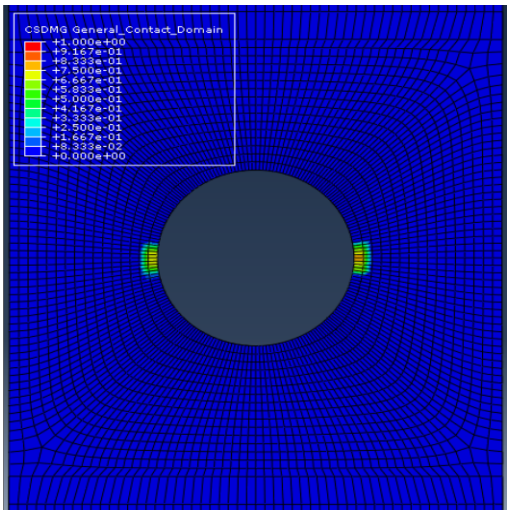

(b) CS damage, Displacement = 0.158709mm

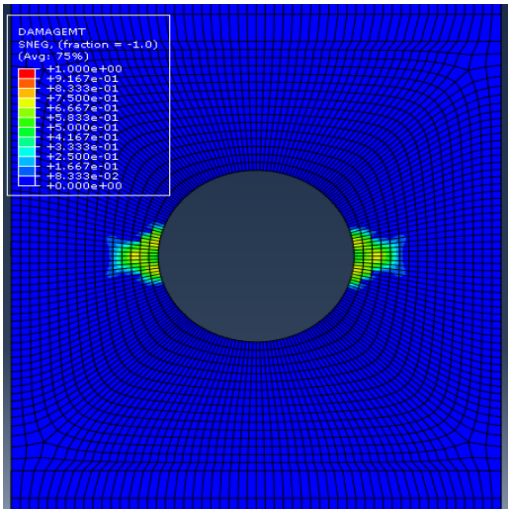

(c) MT damage, Displacement = 0.221832mm

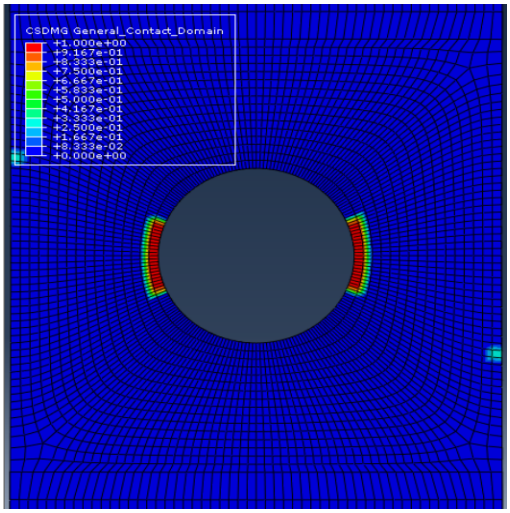

(d) CS damage, Displacement = 0.221832mm

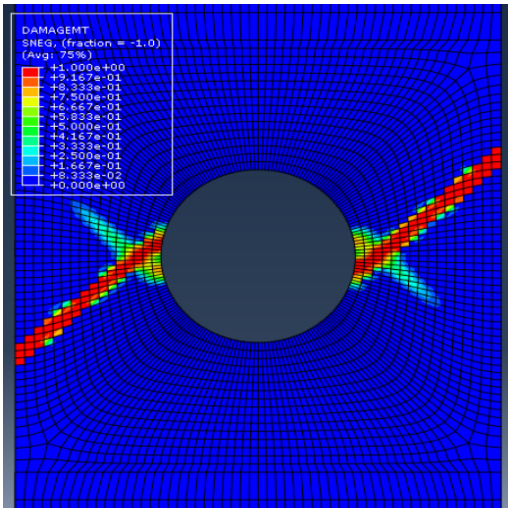

(e) MT damage, Displacement = 0.23114mm

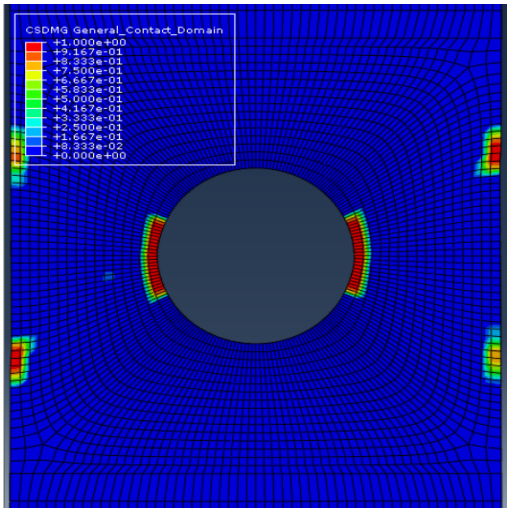

(f) CS damage, Displacement = 0.23114mm

Figure 5.3: Damage evolution up until the failure load

5.3. Comparison to similar research

As mentioned in 3.2, the model in this thesis has the same physical parameters as the computational framework proposed by van der Meer and Sluys [1]. In their work, laminate failure is approached by using interface elements for delamination and eXtended Finite Element Method (XFEM) to model matrix cracking. XFEM is an enrichment of the classical finite element method by extending the solution space of differential equations with discontinuous functions. It enables modelling a mesh-independent representation of discontinuities, like the initiation and evolution of matrix cracks. The key advantage is that it solves the problem discussed in section 5.2. In continuum models local stresses can induce failure in any direction, whereas with XFEM the matrix tensile cracks can be predefined in the $45°$ and $-45°$ direction. This prevents the damage to propagate through the whole thickness of the laminate as illustrated in 5.2.

As can be seen in figure 5.4, the results of van der Meer and Sluys [1] are different in many aspects. This is a consequence of having different failure mechanisms. In the model described in this thesis, the integrity of the laminate is lost when the matrix tensile crack develops through the entire thickness in the same direction. When introducing XFEM in the model, the laminate goes through a whole series of failure mechanisms.
The first failure happens at a displacement of 0.2mm and a load of 1490N. Delamination near the edge of the hole (figure 5.5a), causes a reduction of the effective cross-section that eventually leads to the drop of the load carrying capacity. Afterwards the delamination continues in the interface where loads are transferred up until the moment when the area between the two cracks is fully delaminated.
When the delamination between the cracks is complete, at Failure 2 (figure 5.4), one side of the hole fully separates and causes the snap-back in the graph at a displacement of 0.25mm and a force of 1707N. The dissipation-based arclength method is being used to model the highly dynamic event of this brittle failure. The second snap-back, Failure 3, is caused by the second separation at the other side of the hole. The moment just before this separation is captured in figure 5.5b.

It's now clear that the failure mechanisms of van der Meer and Sluys [1] and the static/dynamic analyses are very different, but failure load of the static analysis corresponds with Failure 1 in figure 5.4. Probably this is just a lucky shot since the failure load of the static analysis still depends largely on the mesh size.
An attempt to match the failure mechanism of van der Meer and Sluys [1] has been made to introduce cohesive cracks in the model. All parameters stayed identical apart from the mesh and the cohesive cracks. The cracks were implemented at the same place as in van der Meer and Sluys [1] and given the surface-based cohesive behaviour. The solution of this analysis resulted in a very low failure load around 1200N. A possible explanation is the generation of the mesh. Since this model is constructed out of 4 parts with odd shapes, it was hard to construct a good mesh. In appendix A.4, the cohesive crack model is given with the results. Since the matrix cracks were predefined the Hashin damage criteria was not used in the analysis.

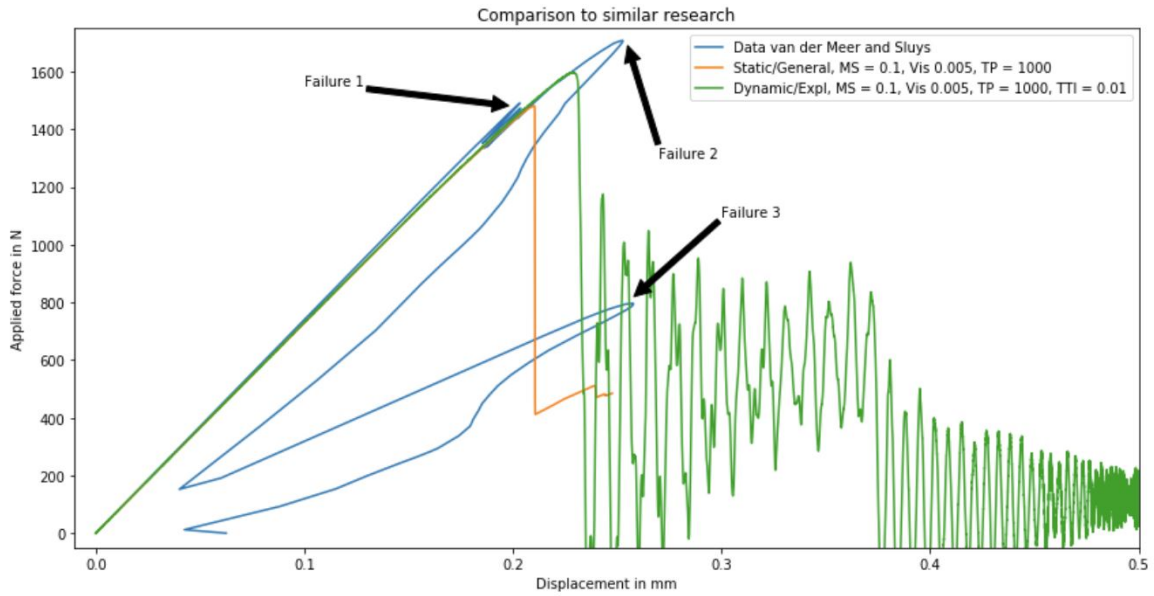

Figure 5.4: Force-displacement diagram comparing static and dynamic analysis to similar research

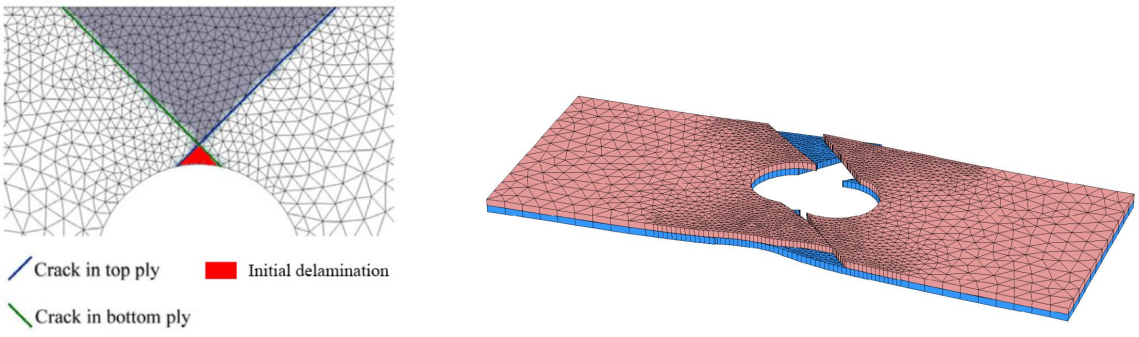

(a) (b)

Figure 5.5: Delamination progress (a) Deformed open-hole tension test just before ultimate failure (b) [2]

6

Conclusions

Modelling delamination in an open-hole tensile test with surface-based cohesive behaviour, has proven to be a challenging task. With the used modelling techniques, non-physical and time parameters have a great influence on the failure loads of Static, General and Dynamic, Explicit analyses. The dynamic solution gives a failure load that is 120 N or 8% higher than the static solution. Both solutions didn't converge to a legitimate failure load due to two reasons:

1. Performing a sensitivity analysis on the target time step of the Dynamic, Explicit analysis, showed that the failure loads for didn't converge to an appropriate value. Investigating the stability of the analyses, demonstrates that a value of 0.01s with a time period of 1000s exhibit a stable solution. Bigger values show inertial effects and very small values, i.e. 0.001s, lead to instability of the solution.
2. Varying the mesh size didn't lead to convergence of the failure loads either. The stability of the analyses was therefore also checked. Taking elements of 0.15x0.15mm and 0.05x0.05mm demonstrate unstable solutions. The range of element sizes between these two, i.e. 0.12mm, 0.1mm and 0.07mm, give stable solutions. Thus the range of possible failure loads for the static analyses lays between the 1440.27-1554.29N for the static analysis and 1557.49-1658.06N for the dynamic analysis. The observed quasi-linear trend in the failure loads, is probably caused by the influence of viscosity regularisation related to the crack band method from Bazant and Oh [15]. This causes bigger elements to loose their stiffness quicker than smaller elements.

To exclude the effects of viscosity regularisation on the results of the static analysis, the ratio of the time period divided by the viscous coefficients has to be set to 200000. Viscosity has shown to have no effect on the dynamic analysis.

Modelling with the surface-based cohesive behaviour technique between the two plies showed to be a very easy-to-use modelling technique. However in the analyses, the delamination did not influence the final failure mode significantly because of the unrealistic failure of both plies at the same cross section, as described below. The advantage of using quasi-static solution obtained by Dynamic Explicit solver, lies in the reduced computation time. The CPU time of the dynamic analysis was 1 hour and 27 minutes and the static analysis 2 hours and 40 minutes where the analysis was aborted in the middle of the imposed displacement of 0.5mm.

Comparing the results of the static and dynamic analysis with the results of van der Meer and Sluys [1], illustrated that the failure loads differ largely. The failure mechanisms are different due homogenisation of the material that is fundamental to continuum models in ABAQUS. At the failure load in the static and dynamic analysis, the matrix fails under tension and shear through the whole thickness of the laminate in the same direction. This unrealistic event differs from the failure mechanism observed in van der Meer and Sluys [1].

6.1. Recommendations

- In order to overcome the unrealistic failure behaviour in the static and dynamic analyses, XFEM modelling techniques can be used to bridge the problem with the damage propagation direction orthogonal to the fibre direction. In the XFEM framework, ABAQUS has the ability to simulate cohesive cracks using an adapted version of the superimposed element formulations.
- An attempt to use a model with cohesive cracks was made unsuccessfully due to the lack of time in this thesis. Further investigation into the technique's capabilities may results in a solution that has the same failure mechanism as observed in van der Meer and Sluys [1].
- Examine if setting the time period of the static analysis very high and the viscosity very low, the influence of the mesh size becomes is smaller. The explanation why the mesh size sensitivity analysis didn't converge remains unanswered. There may be another parameter in ABAQUS that influences the results of different mesh size.
- The choice of the time step of the dynamic analysis wasn't based on the convergence of the results but rather on the stability of the results. Decreasing the time step didn't lead to the convergence of the failure loads. Very small time steps become unstable just before failure in the elastic phase. If these instabilities in the dynamic analysis could be controlled, it may be possible that the failure loads converge.

Bibliography

[1] F. van der Meer and L. Sluys, *Mesh-independent modeling of both distributed and discrete matrix cracking in interaction with delamination in composites,* Engineering Fracture Mechanics **77**, 719 (2010).

[2] F. van der Meer, *Mesolevel modeling of failure in composite laminates: Constitutive, kinematic and algorithmic aspects,* Archives of Computational Methods in Engineering **19**, 381 (2012).

[3] C. Bakis, C. Lawrence, V. Brown, and E. Cosenza, *Fiber-reinforced polymer composites for construction: A state-of-the-art review,* Journal of Composites for Construction **6**, 73 (2002).

[4] L. Ascione, J. Caron, P. Godonou, K. van IJselmuijden, J. Knippers, T. Mottram, M. Oppe, M. Gantriis-Sorensen, J. Taby, and L. Tromp, *Prospect for new guidance in the design of FRP*, Tech. Rep. (Joint Research Centre, Ispra, Italy, 2016).

[5] N. Uddin, *Developments in Fiber-Reinforced Polymer (FRP) Composites for Civil Engineering* (Woodhead Publishing, Cambridge, UK, 2014).

[6] S. Hallett, B. Green, W. Jiang, K. Cheung, and M. Wisnom, *The open hole tensile test: a challenge for virtual testing of composites,* International Journal of Fracture **158**, 169 (2009).

[7] Dassault Système, *Analysis of composite materials with abaqus,* Lecture slides (2009).

[8] D. Gründeman, *Failure analysis of frp joints with abaqus,* Technical university of Delft (2017).

[9] I. Daniel and O. Ishai, *Engineering Mechanics of Composite Materials* (Oxford University Press, New York, 1994).

[10] Dassault Système, *Abaqus documentation,* Retrieved May 28, 2018 ().

[11] S. Tsai, *Strength Characteristics of Composite Materials*, Tech. Rep. (NASA Contractor Reports, Maryland, US, 1965).

[12] S. Tsai and E. Wu, *A general theory of strength for anisotropic materials,* Journal of Composite Materials **5**, 58 (1971).

[13] Z. Hashin, *Failure criteria for unidirectional fiber composites,* Journal of Applied Mechanics **41**, 329 (1979).

[14] P. Camanho, C. Davila, and C. Rose, *Failure criteria for frp laminates,* Journal of composite materials **39**, 323 (2005).

[15] Z. Bazant and B. Oh, *Failure criteria for frp laminates,* Materials and Structures **16**, 155 (1983).

[16] Dassault Système, *Abaqus documentation 31.5.6,* Retrieved May 31, 2018 ().

[17] K. Song, C. Davila, and C. Rose, *Guidelines and Parameter Selection for the Simulation of Progressive Delamination*, Tech. Rep. (NASA Langley Research Center, Maryland, US, 2008).

[18] P. Camanho, C. Davila, and M. Moura, *Numerical simulation of mixed-mode progressive delamination in composite materials,* Journal of composite materials **38**, 1415 (2003).

[19] V. Gaurav, *Constitutive laws for unidirectional composite materials*, Ph.D. thesis, Imperial College London, London, UK (2012).

[20] W. Huaiwen, Q. Qing-Hua, J. Hongwei, and S. Ying, *Comparison among different modeling techniques of 3d micromechanical modeling of damage in unidirectional composites,* Journal of Computational and Theoretical Nanoscience **4**, 400 (2011).

[21] R. Nijsen, *Phenomenological fatigue analysis and life modelling,* Fatigue life prediction of composites and composite structures , 47 (2010).

A
Appendix

A.1. Elastic behaviour

For an orthotropic material 9 independent elastic constants are needed to express the stress-strain relation. The relation is given below.

$$\begin{bmatrix}\epsilon_{11}\\ \epsilon_{22}\\ \epsilon_{33}\\ \gamma_{12}\\ \gamma_{13}\\ \gamma_{23}\end{bmatrix} = \begin{bmatrix} \frac{1}{E_1} & \frac{-\nu_{12}}{E_1} & \frac{-\nu_{13}}{E_1} & 0 & 0 & 0 \\ \frac{-\nu_{12}}{E_1} & \frac{1}{E_2} & \frac{-\nu_{23}}{E_2} & 0 & 0 & 0 \\ \frac{-\nu_{13}}{E_1} & \frac{-\nu_{23}}{E_2} & \frac{1}{E_3} & 0 & 0 & 0 \\ 0 & 0 & 0 & \frac{1}{G_{12}} & 0 & 0 \\ 0 & 0 & 0 & 0 & \frac{1}{G_{13}} & 0 \\ 0 & 0 & 0 & 0 & 0 & \frac{1}{G_{23}} \end{bmatrix} \begin{bmatrix}\sigma_{11}\\ \sigma_{22}\\ \sigma_{33}\\ \tau_{12}\\ \tau_{13}\\ \tau_{23}\end{bmatrix}$$

For transversely isotropic materials it follows that $E_2 = E_3$, $G_{12} = G_{13}$ and $\nu_{12} = \nu_{13}$. This leads to the following compliance relation for transversely isotropic materials.

$$\begin{bmatrix}\epsilon_{11}\\ \epsilon_{22}\\ \epsilon_{33}\\ \gamma_{12}\\ \gamma_{13}\\ \gamma_{23}\end{bmatrix} = \begin{bmatrix} \frac{1}{E_1} & \frac{-\nu_{12}}{E_1} & \frac{-\nu_{12}}{E_1} & 0 & 0 & 0 \\ \frac{-\nu_{12}}{E_1} & \frac{1}{E_2} & \frac{-\nu_{23}}{E_2} & 0 & 0 & 0 \\ \frac{-\nu_{12}}{E_1} & \frac{-\nu_{23}}{E_2} & \frac{1}{E_2} & 0 & 0 & 0 \\ 0 & 0 & 0 & \frac{1}{G_{12}} & 0 & 0 \\ 0 & 0 & 0 & 0 & \frac{1}{G_{12}} & 0 \\ 0 & 0 & 0 & 0 & 0 & \frac{1}{G_{23}} \end{bmatrix} \begin{bmatrix}\sigma_{11}\\ \sigma_{22}\\ \sigma_{33}\\ \tau_{12}\\ \tau_{13}\\ \tau_{23}\end{bmatrix}$$

A.2. Verification

A.2.1. Static, General: time period sensitivity analysis

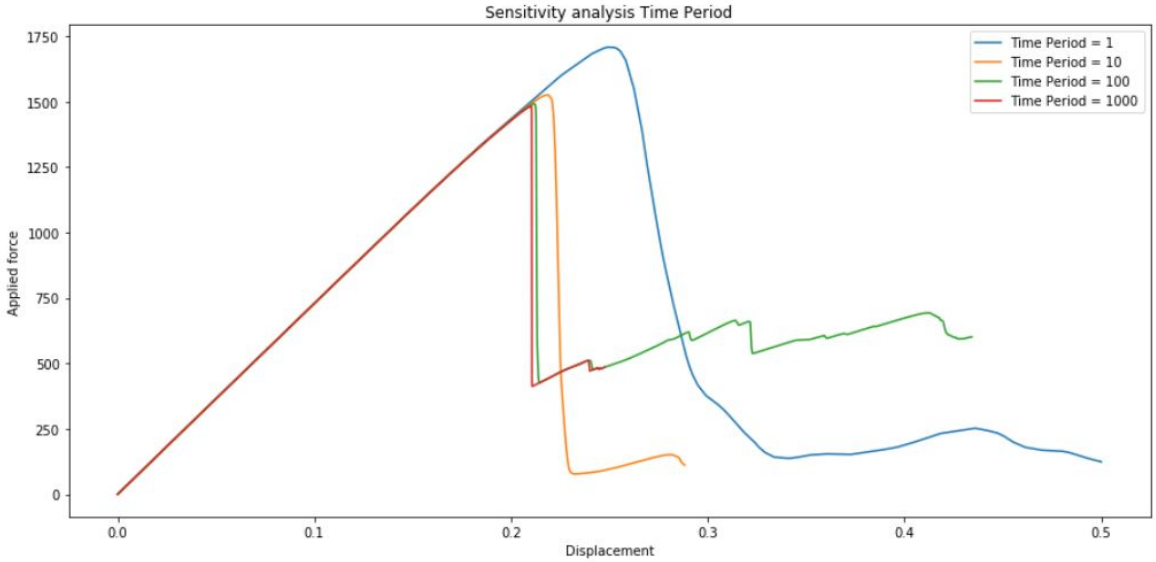

Figure A.1: Force-displacement diagram time period sensitivity analysis

A.2.2. Dynamic, Explicit: time step sensitivity analysis

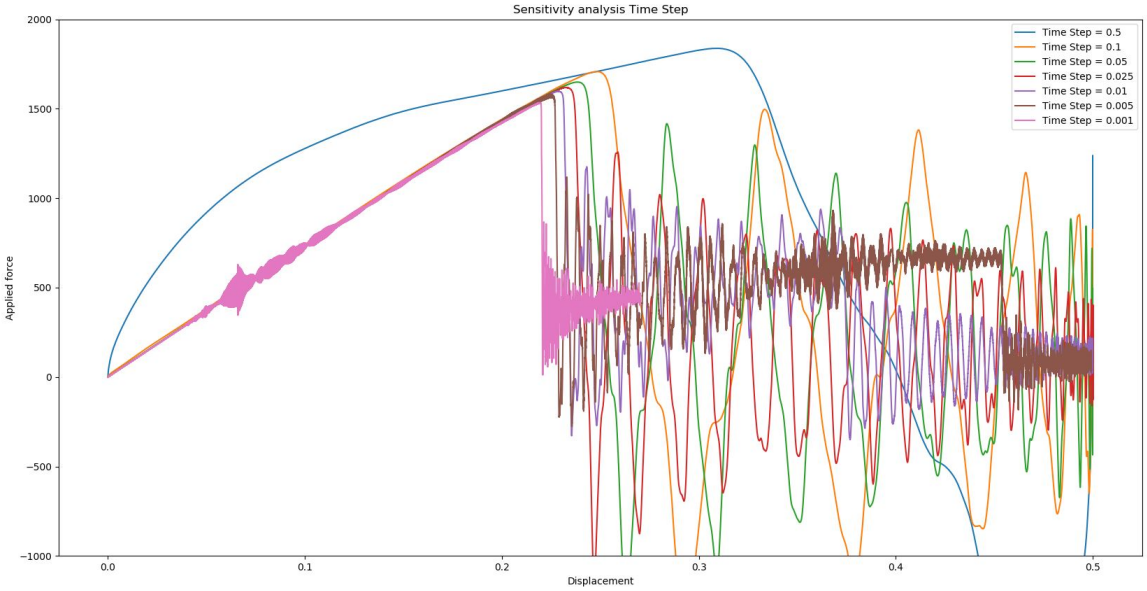

Figure A.2: Force-displacement diagram time step sensitivity analysis

A.2.3. Dynamic, Explicit: time period/time step sensitivity analysis

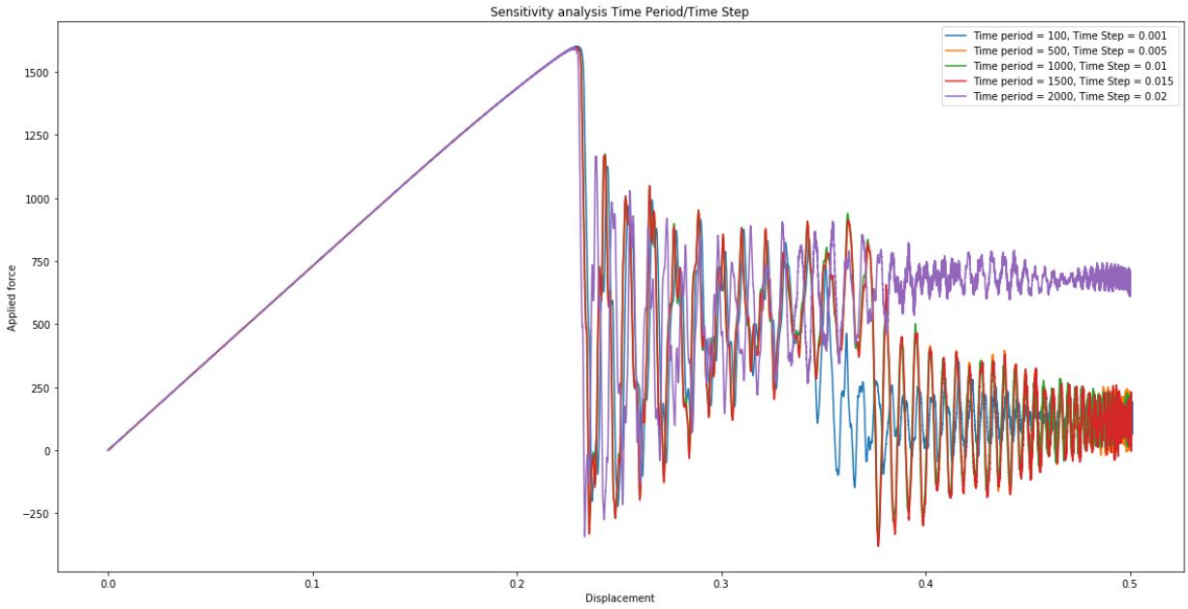

Figure A.3: Force-displacement diagram time period/time step sensitivity analysis

A.2.4. Mesh size sensitivity analysis

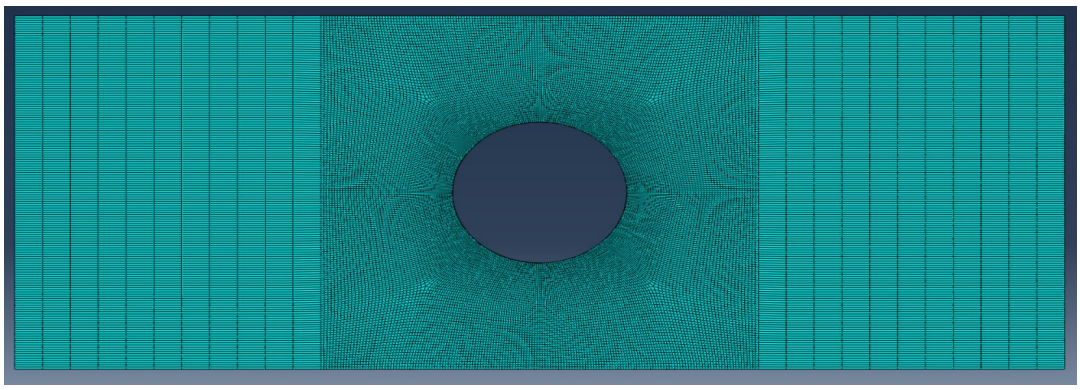

Figure A.4: Mesh size 0.05mm

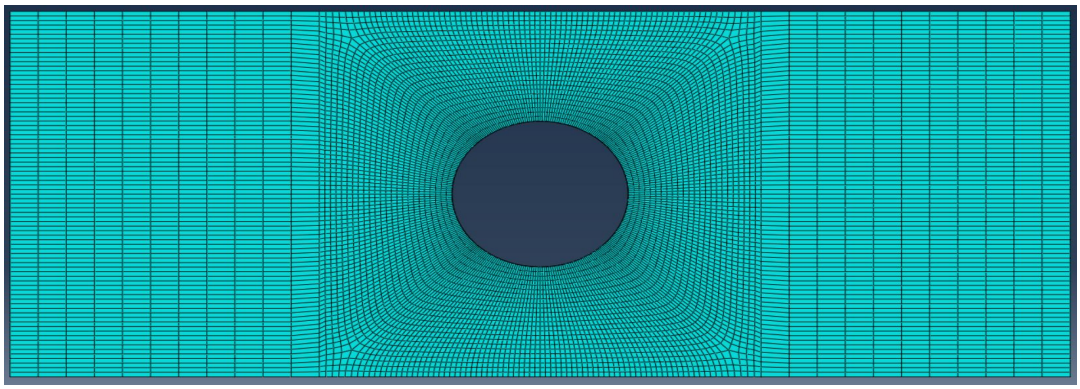

Figure A.5: Mesh size 0.07mm

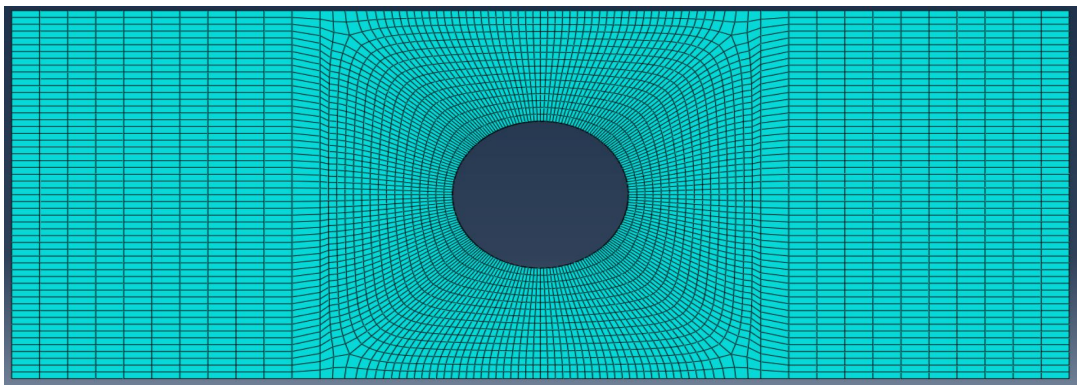

Figure A.6: Mesh size 0.1mm

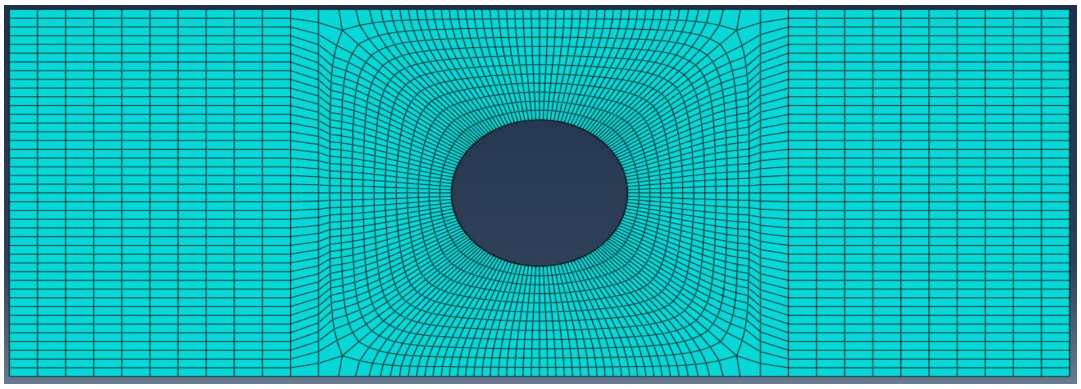

Figure A.7: Mesh size 0.12mm

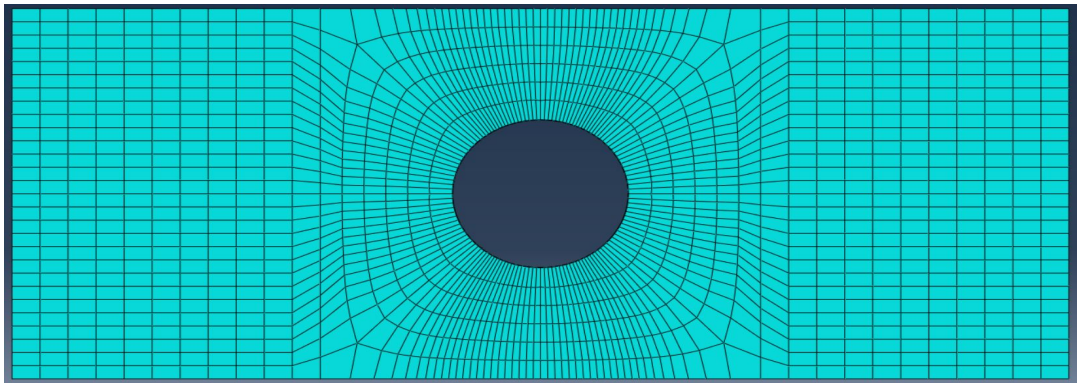

Figure A.8: Mesh size 0.15mm

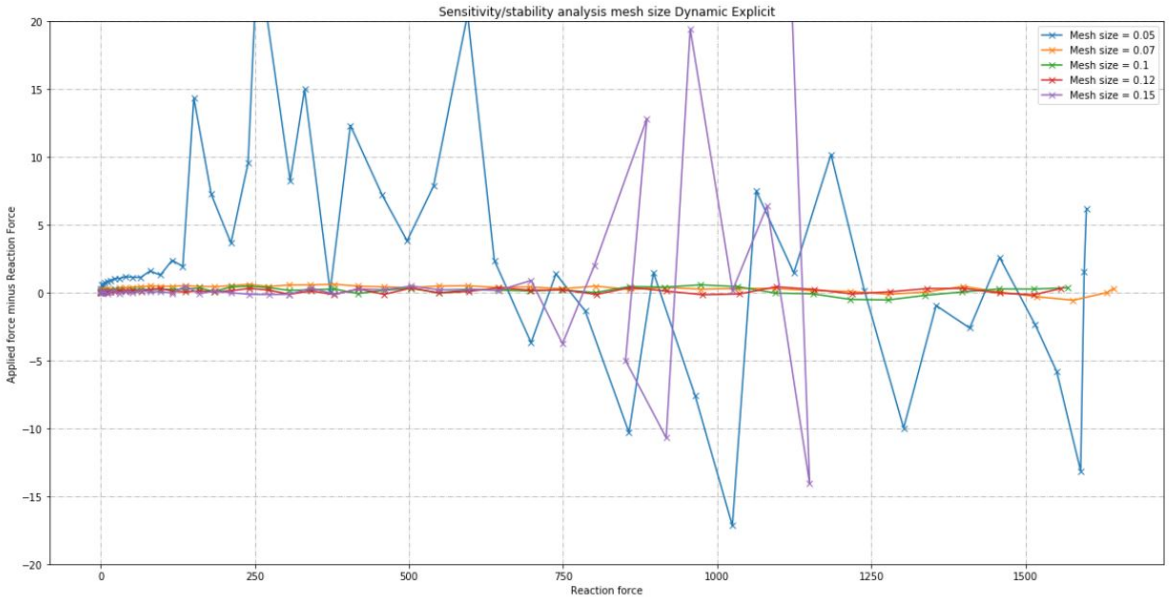

Figure A.9: Mesh size stability analysis

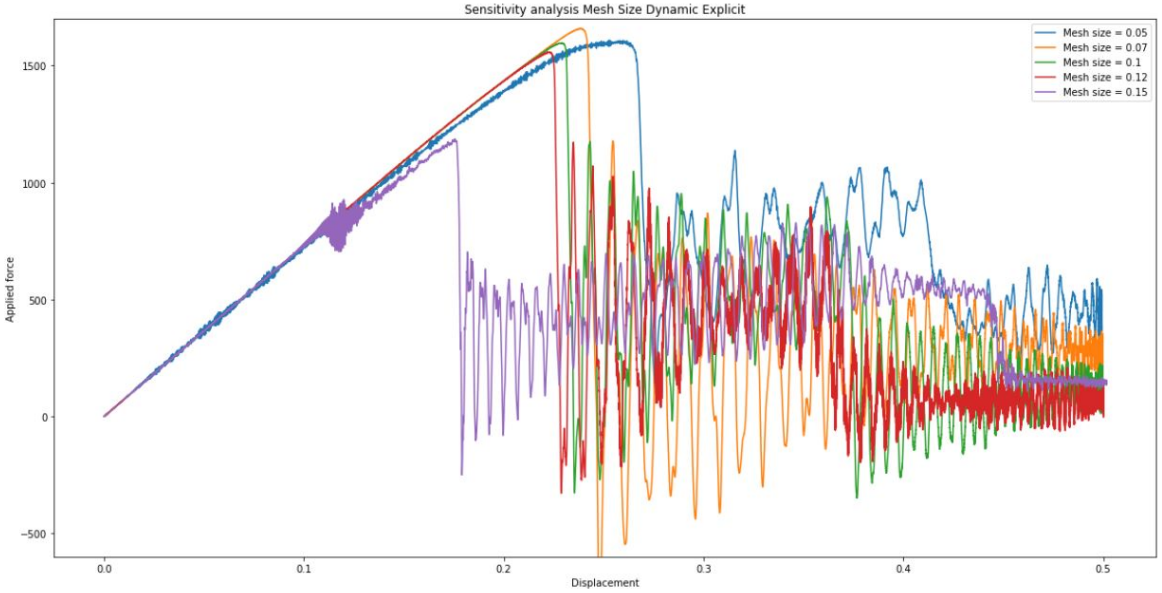

Figure A.10: Force-displacement diagram mesh size stability analysis

A.3. Damage propagation

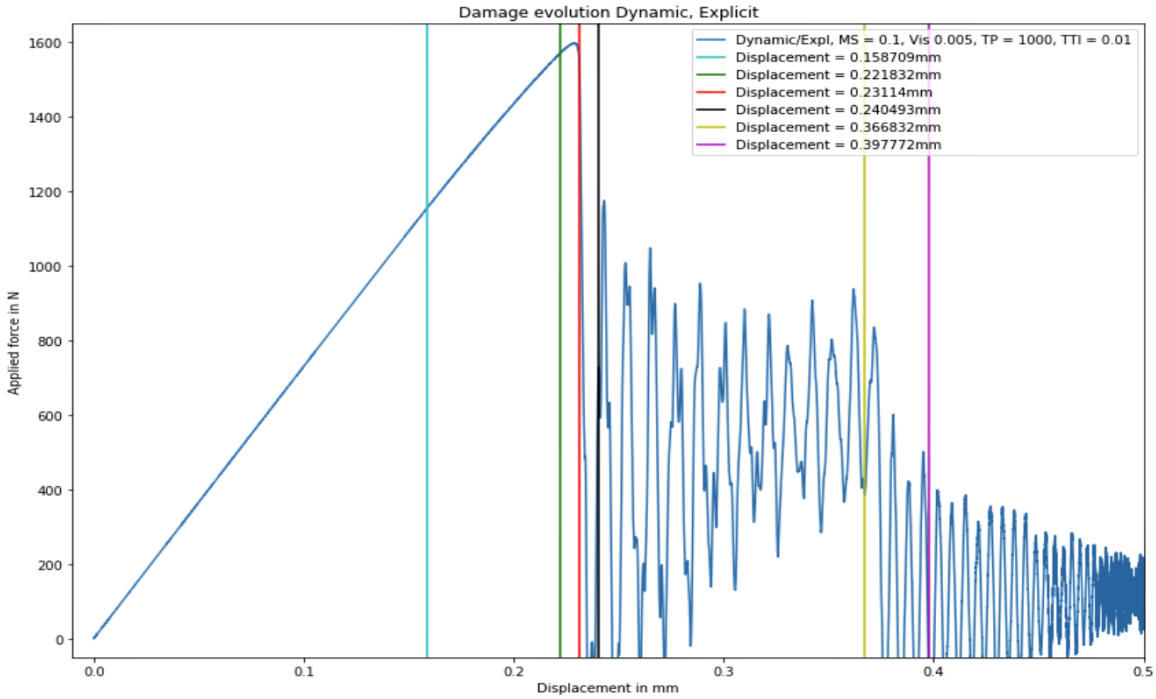

Figure A.11: Force-displacement diagram displaying all the damage frames in figure 5.3 and A.12

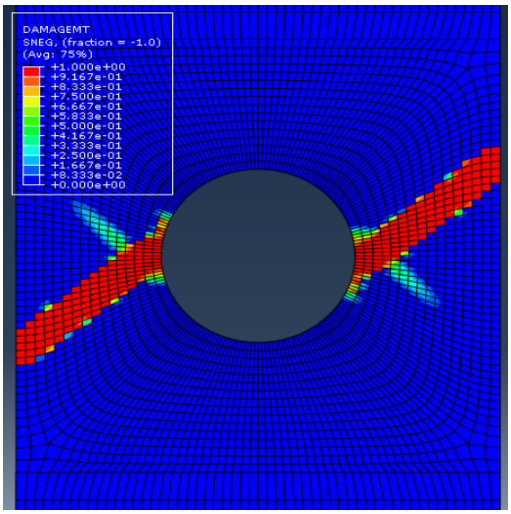

(a) MT damage, Displacement = 0.240493mm

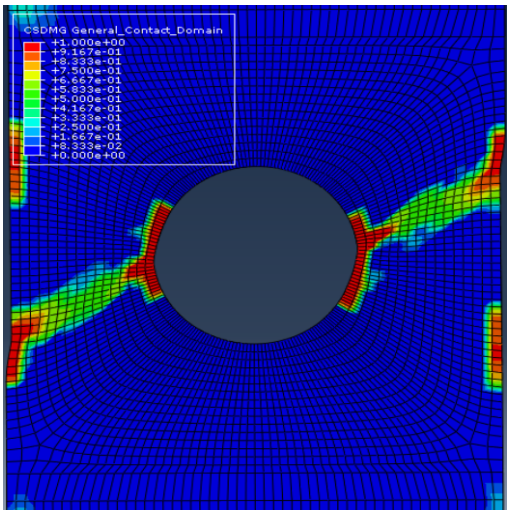

(b) CS damage, Displacement = 0.240493mm

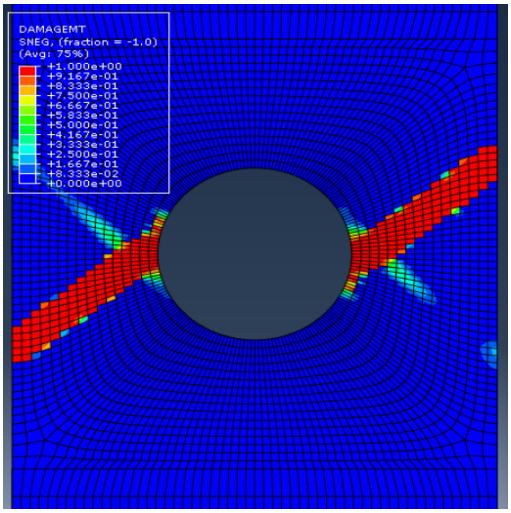

(c) MT damage, Displacement = 0.366832mm

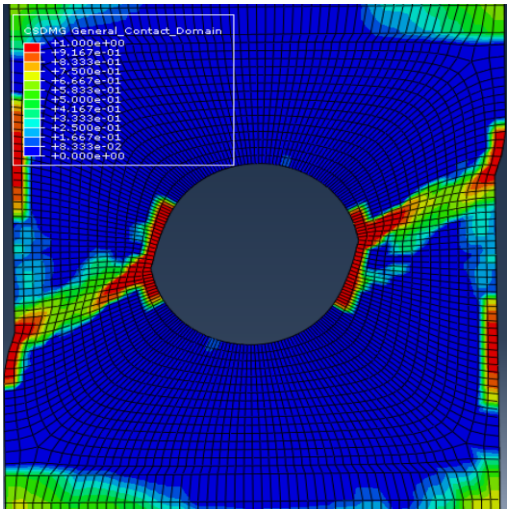

(d) CS damage, Displacement = 0.366832mm

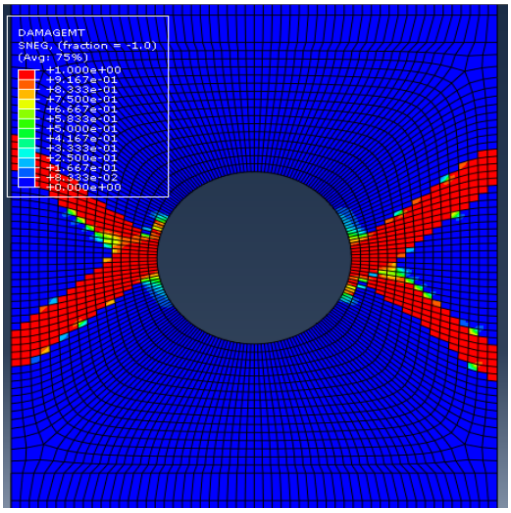

(e) MT damage, Displacement = 0.397772mm

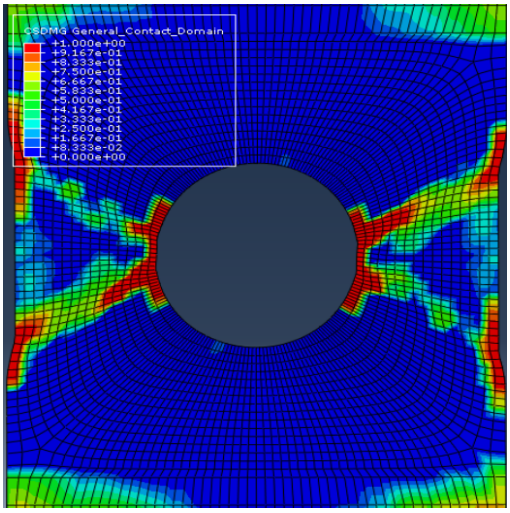

(f) CS damage, Displacement = 0.397772mm

Figure A.12: Damage evolution after the failure load

A.4. Cohesive cracks model

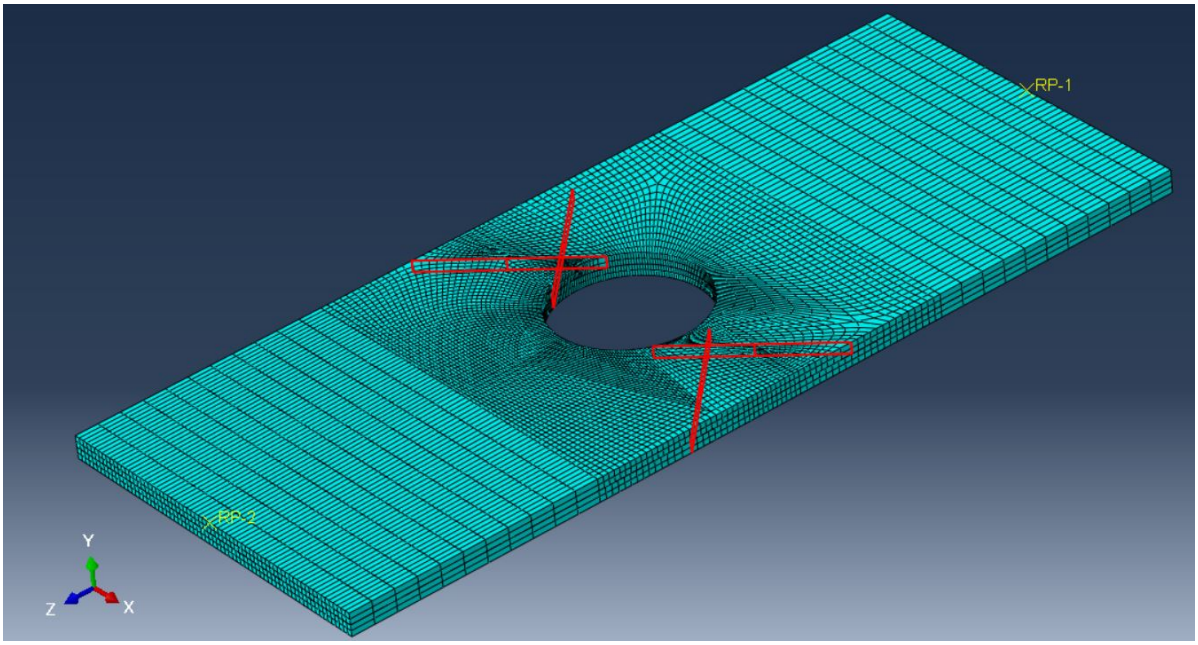

Figure A.13: Cohesive crack model displaying the location of the cracks in red

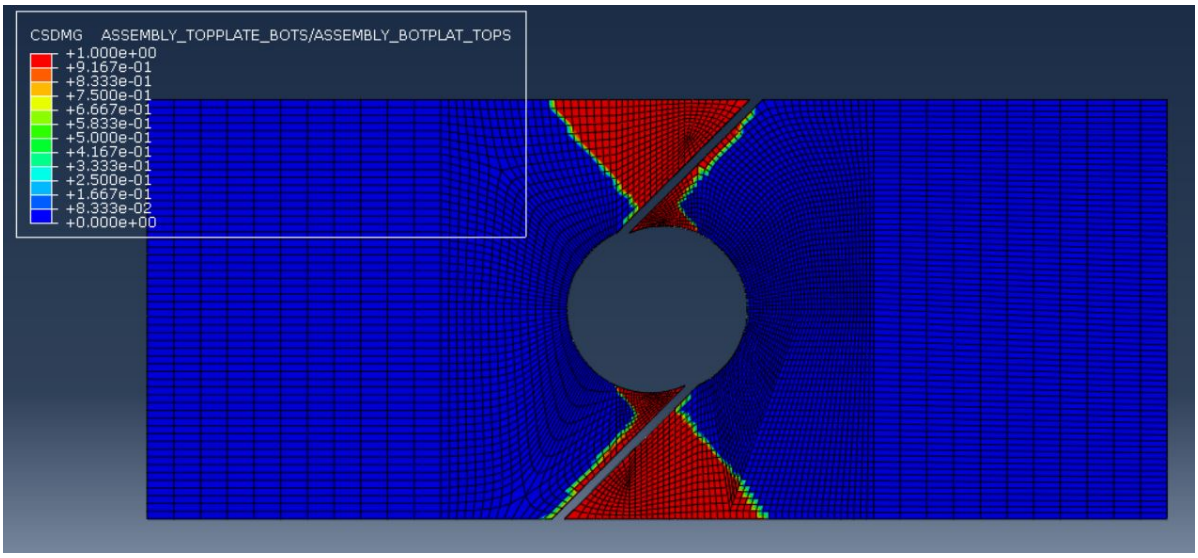

Figure A.14: Cohesive crack model at a displacement of 0.5mm with the delamination coloured in red

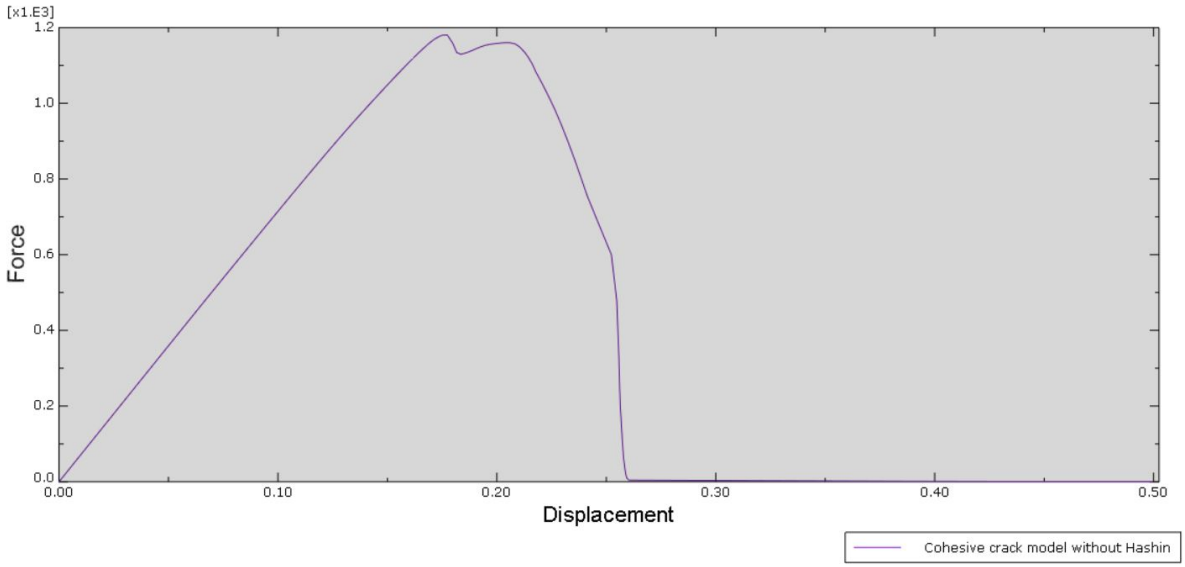

Figure A.15: Force-displacement diagram for cohesive crack model

A.5. Project plan

Brief description

The topic of my bachelor thesis will be modelling an open hole tension test of fibre reinforced polymers (FRP) in Abaqus, a finite element analysis (FEA) computer programme. Previously, a student already tried to model this test but did not succeed in modelling delamination and matrix cracking in the same model. The goal of the project is to find a good modelling method with Abaqus to approximate the failure behaviour of a $[45/-45]$ layup of FRP in a open hole tension test. The results of the tests in Abaqus will be benchmarked with prior research and possibly experiments in the Stevin lab.

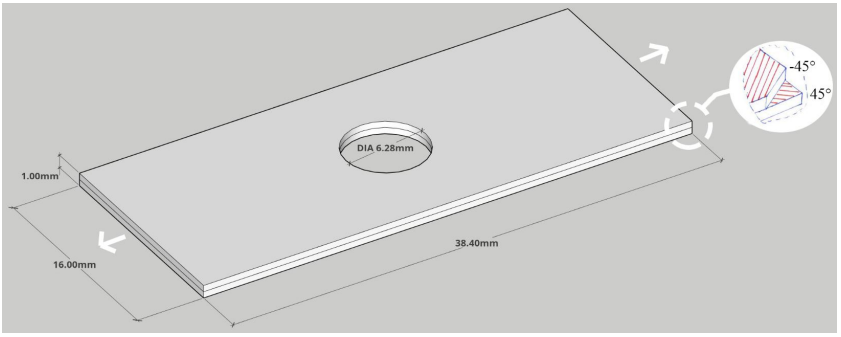

Figure A.16: Situational sketch

As mentioned before, a finite element analysis will be performed to solve the FRP open hole test. Since Abaqus is one of the most widely used programs for FEA, it is probably suitable to reach the goal of this thesis. The ability of the program to define cohesive properties for delamination and ply failure for matrix cracking and fibre failure will be examined. It will be necessary to discuss different modelling techniques and compare results to achieve an optimal technique.

The final report will begin with a short introduction on FRP materials and their modelling techniques. Then followed by a description of the modelling approaches and validation, the results of the models, subsequently the discussion of the results and finally the conclusion.

Why this subject?

The choice for this thesis, three major factors had a role. First of all, I've always been fascinated by finite element models. Sadly, we never had the opportunity in the bachelor to explore the subject of finite element analysis. Therefore I saw this thesis as an ideal moment to pursue my interest.
Secondly, in my bachelor of civil engineering, I didn't spend a lot of time studying materials and their characteristics. In the courses of Structural Mechanics a small basis was given to understand the theory of relating material properties to stress and strain. This really interested me and and I understood it well. Since FRP is getting more accepted as a construction material, my interest grew even bigger.
Finally, I recently decided to follow the master Structural Engineering. Before I was heavily hesitating between Structural and Building Engineering but the lack of theory in the Building Engineering lead to my choice of today. I think that by choosing a structural engineering thesis I will get better arguments for my choice.
Due to modest knowledge in FEA and laminate theory, I see this thesis as a challenge where I will explore new subjects and experiences.

Planning

In table A.1, you can find a preliminary planning. The thesis will consist of 10 weeks with an extra week if improvements to the report will be necessary.

Table A.1: Coarse planning BSc thesis

Weeknumbers	1	2	3	4	5	6	7	8	9	10	11
1. Project planning, start meeting CiTG											
2. Installing Abaqus											
3. Literature study on laminate theory											
4. Experimenting with Abaqus + create set-up report											
5. Elaborate moddeling approaches											
6. Creating first models and have first results											
7. Fine-tune models											
8. Evaluate results											
9. Finishing report											
10. Presentation											
11. Corrections report if necessary											

Milestones:

- Start meeting: 23/04/2018
- Kick-off meeting Marko & Frans: 30/04/2018
- Intermediate report: 18/05/2018
- Hand-in final report: 18/06/2018
- Presentation: 25/06/2018
- Correction deadline: 02/07/2018